Accepted Manuscript

Geological Society, London, Memoirs

Antarctic Palaeotopography

Guy J. G. Paxman

DOI: https://doi.org/10.1144/M56-2020-7

To access the most recent version of this article, please click the DOI URL in the line above. When citing this article please include the above DOI.

Received 2 February 2020
Revised 5 May 2020
Accepted 28 June 2020

Antarctic Palaeotopography

Guy J. G. Paxman[1,2]
[1] Department of Geography, Durham University, Durham, UK
[2] Lamont-Doherty Earth Observatory, Columbia University, New York, USA
gpaxman@ldeo.columbia.edu

Abstract

The development of a robust understanding of the response of the Antarctic Ice Sheet to present and projected future climatic change is a matter of key global societal importance. Numerical ice sheet models that simulate future ice sheet behaviour are typically evaluated with recourse to how well they reproduce past ice sheet behaviour, which is constrained by the geological record. However, subglacial topography, a key boundary condition in ice sheet models, has evolved significantly throughout Antarctica's glacial history. Since mantle processes play a fundamental role in the generation and modification of topography over geological timescales, an understanding of the interactions between the Antarctic mantle and palaeotopography is crucial for developing more accurate simulations of past ice sheet dynamics. This chapter provides a review of the influence of the Antarctic mantle on the long-term evolution of the subglacial landscape, through processes including structural inheritance, flexural isostatic adjustment, lithospheric cooling and thermal subsidence, volcanism and dynamic topography. The uncertainties associated with reconstructing these processes through time are discussed, as are important directions for future research and the implications of the evolving subglacial topography for the response of the Antarctic Ice Sheet to climatic and oceanographic change.

1. Overview

1.1. Unveiling the subglacial landscape of Antarctica

Antarctica is unique among Earth's continents in that the crust is almost entirely capped by a layer of ice up to 4 km thick. Today, ~99.8% of the Antarctic landmass is concealed beneath the Antarctic Ice Sheet (AIS) (Burton-Johnson et al., 2016), and this figure was likely even larger during recent glacial maxima (Bentley et al., 2014). The near-total lack of exposure of the Antarctic 'land surface' presents major challenges for understanding the long-term history of the AIS.

The progressive mapping of Antarctica's subglacial topography has been driven by a substantial community effort since the 1970s (Drewry, 1983; Fretwell et al., 2013; Lythe et al., 2001; Morlighem et al., 2019; Schroeder et al., 2019). Ground-based and airborne radio-echo sounding (RES) surveys are widely used to measure ice thickness in Antarctica. Although minor differences exist between the radar systems that have been employed in Antarctica, they share a common basic premise. An electronic signal is converted to radio waves, which are emitted from an antennae array mounted on the survey platform (e.g. aircraft). This radar pulse propagates through the air and ice sheet, and energy is reflected at interfaces with strong acoustic impedance contrasts (Figure 1). The strongest reflections are from the air-ice and ice-bed interfaces; weaker reflections are also seen from internal layers within the ice. Upon their return to the carrier platform, the echoes are detected by a receiver

and converted back to an electronic signal. The system then records the time delay between the pulse being emitted and received – the two-way travel time.

The ice surface and bed reflectors are extracted ('picked') from each radar trace (Figure 1). The difference in the two-way travel times of these two reflectors gives the two-way travel time of the radar in the ice, which is multiplied by an assumed radar velocity in ice (~168 m/μs), with an additional small correction commonly made for the firn layer (the thin layer of snow and uncompacted ice at the top of the ice sheet, which does not generate strong radar reflections) to give the ice thickness. The difference between the ice surface elevation (which can be determined via laser altimetry) and the ice thickness gives the bed elevation. Location and altitude of the radar platform are determined using a global positioning system (GPS).

Up to 2013, ~25 million ice thickness measurements (Figure 1) had been acquired and incorporated into the Bedmap2 digital elevation model (DEM) of Antarctica's bedrock topography (Figure 2) (Fretwell et al., 2013). However, approximately only one third of cells within Bedmap2 contain at least one real ice thickness measurement (the grid is at 5 km horizontal resolution), and some areas are >200 km away from the nearest real data point (Fretwell et al., 2013). Several multi-season field campaigns have commenced since the publication of Bedmap2, with the aim of filling some of these major data gaps (Figure 1).

1.2. Bed topography and ice sheet behaviour

Antarctica's subglacial topography is important to our understanding of AIS history. It has become increasingly recognised that subglacial topography exerts a fundamental influence on the dynamics of the overlying ice sheet (Austermann et al., 2015; Colleoni et al., 2018; Gasson et al., 2015; Wilson et al., 2013), and is therefore an important boundary condition in numerical ice sheet models. Ice sheet models aim to simulate the present dynamics of the AIS and predict the response of the ice sheet to future projected climatic change, and in turn evaluate likely changes in global sea levels (DeConto and Pollard, 2016; Edwards et al., 2019; Golledge et al., 2015; Mengel and Levermann, 2014). Since bed topography exerts a strong influence on ice sheet dynamics, it is important for any ice sheet model to incorporate an accurate DEM of present-day subglacial topography.

Of particular significance are 'marine ice sheets', which are grounded on bed situated below sea level. Marine ice sheets that are grounded on an inland-dipping ('reverse sloping') bed are hypothesised to be particularly susceptible to perturbations in atmosphere and ocean temperatures (Mercer, 1978; Thomas, 1979). In this scenario, when the grounding line of the marine ice sheet retreats, it retreats into deeper water, leading to increased flotation, basal melting, and ice discharge, resulting in further retreat and a self-sustained positive feedback (Schoof, 2007). This process is known as marine ice sheet instability, and permits a highly non-linear response of the grounding line to initial climate and ocean forcing, creating the possibility of rapid retreat or even catastrophic collapse of marine-based ice sheets (Joughin and Alley, 2011; Mercer, 1978; Scherer et al., 1998; Schoof, 2007; Thomas, 1979). Ice sheet modelling studies incorporating marine ice sheet instability processes (Pollard et al., 2015) have predicted global sea level rise of ~1 metre by the end of the current century (DeConto and Pollard, 2016). However, probabilistic model projections indicate that these values may significantly overestimate the rate of ice mass loss and sea level rise (Edwards et al., 2019). Moreover, a number of processes have been documented that may act to

counteract marine ice sheet instability, such as slow ice shelf removal rates (Clerc et al., 2019), local isostatic uplift of the bed beneath the grounding line (Barletta et al., 2018; Kingslake et al., 2018), and deformation-induced relative sea level change (Gomez et al., 2010).

Marine-based ice in Antarctica has the potential to contribute ~23 m of global sea level rise (Fretwell et al., 2013); the amount of warming required to induce significant retreat of marine-based parts of the ice sheet, and the likely rate and magnitude of the retreat, are therefore questions of crucial societal importance. In order to constrain these unknowns, attention has focussed on records of AIS stability during past warm periods in Earth's history that may serve as analogues for future climate conditions. Ice sheet models are typically assessed by how well they can reproduce past ice sheet behaviour (as constrained from geological and sea level records) before they can be confidently used to predict the response of the AIS to projected future climate scenarios. Since certain areas of the subglacial topography of Antarctica have been extensively modified since glacial inception ca. 34 million years ago (Jamieson et al., 2010; Paxman et al., 2019b; Pollard and DeConto, 2019; Wilson et al., 2012), it is unrealistic to use the modern bed topography when attempting to model early Antarctic ice sheets. Using a more realistic reconstruction of subglacial topography for past time intervals has the potential to increase the robustness of ice sheet model results, and in turn (a) facilitate improved understanding of the response of past Antarctic ice sheets to climatic change (DeConto and Pollard, 2003a; Wilson et al., 2013) and (b) engender greater confidence in projections of future ice sheet stability, mass loss, and sea level change.

Additionally, the morphology of subglacial topography is an important repository of information pertaining to past ice sheet dynamics. A landscape contains a record of the processes that have acted to shape it, and Antarctic geomorphology studies typically aim use age relationships and the morphology of landscape features to determine the history of the landscape and the processes that produced it. This analysis can reveal insights as to the spatial extent, dynamics and behaviour of past ice sheets, in particular during past warmer climate intervals potentially analogous to the future. For example, RES data have revealed subglacial landforms and areas of enhanced glacial erosion within the Aurora Subglacial Basin in East Antarctica, several hundred kilometres inland of the modern ice margin (Aitken et al., 2016; Young et al., 2011). Such landforms likely formed near the margin of a dynamic early ice sheet with a more restricted extent than at the present-day.

1.3. Antarctic glacial history

The timescales over which changes in Antarctic bed topography are most significant in this context are intrinsically linked to the intervals during which ice sheets have been present in the Southern Hemisphere. Marine oxygen isotope records indicate that the Earth has been experiencing a long-term cooling trend since the Early Eocene Climatic Optimum (ca. 51 Ma; Figure 3) (Zachos et al., 2001). The first appearance of continental-scale ice sheets in Antarctica is widely agreed to have occurred around the time of the Eocene–Oligocene boundary (ca. 34 Ma) (Coxall et al., 2005; Liu et al., 2009; Zachos et al., 2001), which marks the transition between the 'greenhouse world' of the Cretaceous–Eocene and the 'icehouse world' that Earth has inhabited since the start of the Oligocene (Figure 3). Stratigraphic records indicate that ice sheet growth occurred in a stepwise fashion across the Eocene–Oligocene transition, in concert with the marine oxygen isotope record (Coxall et al., 2005; Katz et al., 2008; Passchier et al., 2017; Scher et al., 2011). However, it is important to note that although this climate transition marks the first appearance of large-scale

Southern Hemisphere ice sheets, ephemeral ice sheets and/or mountain glaciers may have existed on Antarctica at an earlier stage (Carter et al., 2017).

The mechanisms behind the precise timing of glacial inception in Antarctica remain subject to continuing debate. However, it is widely believed that continental-scale glaciation on Antarctica was triggered by a drop in atmospheric pCO_2 levels below a threshold (DeConto et al., 2008; DeConto and Pollard, 2003a; Pagani et al., 2011; Pearson et al., 2009) combined with associated internal feedbacks within the carbon cycle (Reusch, 2011; Scher et al., 2011; Tripati et al., 2005; Zachos and Kump, 2005). The opening/deepening of ocean gateways around Antarctica, in particular the Drake Passage and the Tasman Gateway, may have also played a role in the timing of glaciation (DeConto and Pollard, 2003b; Kennett, 1977).

Cyclicity in marine oxygen isotope and sedimentary records from drill cores around the Antarctic margin indicates that the early Antarctic ice sheets waxed and waned in concert with orbital cycles during the Oligocene and early Miocene (Barrett, 2008; Hambrey et al., 1991; Naish et al., 2001; Zachos et al., 2001, 1997). Approximately 33 glacial cycles have been detected in this interval, and the sedimentary record suggests that meltwater was abundant, with conditions similar to present-day Greenland (Naish et al., 2001; Sugden and Jamieson, 2018). Marine sediment cores from the Ross Sea revealed an erosional hiatus at the Oligocene–Miocene boundary (ca. 23 Ma) indicative of a major episode of global cooling and ice sheet expansion (Naish et al., 2001), which has also been inferred from a contemporaneous benthic foraminiferal oxygen isotope shift that implies a significant increase in ice volume (Figure 3) (Zachos et al., 2001). Following the mid-Miocene Climatic Optimum, a gradual cooling trend commenced at ca. 14 Ma (Figure 3). Decreasing air and ocean temperatures allowed the AIS to expand significantly under an arid polar climate (Zachos et al., 2001), and the oscillatory and more restricted ice masses evolved into a major and persistent continental ice sheet (Figure 3) (DeConto and Pollard, 2003a; Jamieson et al., 2010). The ice sheet extended to the continental shelf edge, perhaps on multiple occasions, before retreating and stabilising with dimensions similar to that of the present-day (Sugden and Denton, 2004).

This multi-faceted glacial history over the past 34 million years provides a large window of time for significant topographic and landscape evolution to occur in Antarctica. Efforts to understand palaeotopography in Antarctica have therefore primarily focussed on the time period from glacial inception at ca. 34 Ma to the present-day (Jamieson and Sugden, 2008; Paxman et al., 2019b; Wilson et al., 2012; Wilson and Luyendyk, 2009). However, attempts are also ongoing to produce reconstructions of Antarctic palaeotopography during the early Cenozoic and Late Cretaceous, which will be important boundary conditions for the modelling of older ice masses, regional ocean and atmosphere circulation, and palaeoclimate.

1.4. Framework of landscape evolution in Antarctica

Landscape evolution reflects the competition between ‘solid Earth’ processes such as tectonics, which act to increase or decrease the elevation of the crust, and ‘Earth surface’ processes such as erosion and sedimentation, which modify it. In Antarctica, the mantle facilitates the generation of surface topography via:

1. The flexural isostatic response to load redistribution (via e.g. erosion, sedimentation, movement on faults), which is governed by the balance of forces in the crust and mantle lithosphere and causes uplift or subsidence of the Earth's surface.
2. Heating or cooling of the lithosphere, which alters the density of the crust/mantle lithosphere and drives a transient phase of surface uplift or subsidence. Heating can also induce volcanic activity, causing emplacement of magmatic material on the Earth's surface or intrusion of magmatic material within the crust.
3. Viscous normal tractions applied to the base of the lithosphere by density-driven convective flow within the mantle ('dynamic topography').

Each of these processes (Figure 4) is to a greater or lesser extent influenced by the properties of the mantle, and are described in turn in the following sections of this chapter.

2. Isostasy

2.1. Elastic plate flexure

Isostatic adjustment occurs in response to the redistribution of loads on the surface of, or within, the lithosphere on wavelengths of order 100–1000 km. Landscape evolution processes involve the redistribution of surface and sub-surface material on these length scales, and therefore induce vertical surface displacement via the isostatic re-equilibration of the lithosphere. Moreover, isostasy is the process by which many solid Earth phenomena cause changes in surface topography, and is therefore the most ubiquitous link between mantle properties and landscape evolution processes (Figure 4).

The flexural isostatic model states that surface and sub-surface loads are supported by a combination of (a) buoyancy forces imparted on the base of the crust by the mantle lithosphere, which arise due to the difference in density between crust and mantle (Airy isostasy), and (b) elastic bending forces within the lithosphere. The ratio of buoyancy forces and elastic bending forces is a function of the wavelength of the load and also the flexural rigidity of the lithosphere. The flexural response of the lithosphere to (un)loading over geological timescales (>10^6 years) may be computed by modelling the lithosphere as a thin elastic plate overlying an inviscid (non-viscous) substrate (the asthenospheric mantle) (Watts, 2001; Watts et al., 2013). The general two-dimensional flexure equation giving the downward deflection (w) of the elastic plate in response to loading (h) is given by

$$\nabla^2[D(x,y)\nabla^2 w(x,y)] + (\rho_{mantle} - \rho_{infill})gw(x,y) = (\rho_{load} - \rho_{displace})gh(x,y) \quad (1)$$

where

$$D(x,y) = \frac{ET_e(x,y)^3}{12(1-\nu^2)} \quad (2)$$

is the flexural rigidity of the lithosphere as a function of spatial dimensions x and y. E (Young's modulus; 100 GPa) and ν (Poisson's ratio; 0.25) are elastic constants and the density terms (ρ) depend on the particular loading or unloading scenario being considered. The densities of the load and the mantle are given by ρ_{load} and ρ_{mantle} respectively. The terms for $\rho_{displace}$ and ρ_{infill} can be

ignored for subaerial surface loads, but for subaqueous loads the density contrasts between (i) the load and the displaced water, and (ii) the mantle and the material filling in the flexural moat (e.g. water, sediment) must also be included.

The spatial pattern (amplitude and wavelength) of the flexural isostatic response to (un)loading is determined by the flexural rigidity (D) or its proxy, the effective elastic thickness (T_e) of the lithosphere (Watts, 2001). T_e is a measure of the equivalent thickness the lithosphere would have if it behaved as a perfectly elastic plate overlying an inviscid fluid asthenospheric mantle, as is assumed by the thin elastic plate model (Equation 2). In reality, the composition and rheology of the lithosphere is strongly heterogeneous, so T_e is more appropriately conceptualised as a proxy for the depth-integrated strength of the lithosphere (Watts and Burov, 2003). An important implication of the flexure model is that provided the lithosphere has a finite rigidity/strength, vertical surface displacement occurs beyond the spatial limits of the (un)load (Figure 4); flexural isostasy is therefore known as 'regional isostasy'.

2.2. Flexural rigidity of the Antarctic lithosphere

Flexurally rigid lithosphere is associated with long-wavelength, low-amplitude flexural displacement, whereas flexurally weak lithosphere is associated with short-wavelength, high-amplitude flexural displacement. Since the effective elastic thickness governs the pattern of flexural adjustment to load redistribution, the depth-integrated strength of the Antarctic lithospheric mantle is an important parameter in landscape evolution models. Attempts to estimate T_e in Antarctica can be divided into two broad categories.

1. Forward modelling techniques, whereby an observed manifestation of flexure such as a deflected/warped topographic surface and/or its associated gravity anomaly is compared to the predictions of an elastic plate model in which T_e can be adjusted. The value of T_e in the model that yields the best fit with the observed flexure is regarded as the estimate of T_e at the time of loading for the region under consideration. Such methods have recovered T_e values of 5±5 km for parts of the West Antarctic Rift System (Jordan et al., 2010; Wenman et al., 2020), ~5 km close to the front of the Transantarctic Mountains, increasing to ~85–115 km beneath the Wilkes Subglacial Basin (Stern et al., 2005; Stern and ten Brink, 1989; ten Brink et al., 1997), and 20–25 km in the Recovery Basin (Paxman et al., 2017) (Figure 5a).
2. Inverse (spectral) modelling of observed gravity anomalies and subglacial topography. The two spectral parameters commonly used to estimate T_e from gravity and topography data are the free-air admittance and the Bouguer coherence. The free-air admittance is the linear transfer function between the free-air anomaly and the topography in the frequency domain, while the Bouguer coherence is essentially the square of the Pearson product-moment correlation coefficient between the Bouguer gravity anomaly and the topography, again computed in the frequency

domain (Kirby, 2014). The forms of these two spectral parameters as a function of wavelength can be used to estimate T_e, and have recovered values of ~35 km in the Weddell Sea embayment (Studinger and Miller, 1999), ~10 km in the Gamburtsev Subglacial Mountains (Paxman et al., 2016) and ~20 km in the Recovery Basin (Paxman et al., 2017) (Figure 5b).

While the forward modelling methods are robust where a clear surface manifestation of flexure, such as tilted palaeo-land surfaces, can be discerned (Paxman et al., 2017; ten Brink et al., 1997), reference surfaces with a known geometry prior to flexural warping are rarely identified in Antarctica given the lack of surface exposure. In addition, forward models recover the T_e pertaining to the time at which loading occurred, which is not necessarily equivalent to the contemporary T_e. The ability of T_e to evolve over geological timescales (e.g. Watts et al., 2013), has been documented for the rifted basins in the Ross Sea (Karner et al., 2005). The potential temporal variation of T_e adds an additional level of uncertainty in reconstructing flexure in Antarctica over long timescales.

By contrast, the inverse spectral methods can be applied over large areas, since most of Antarctica has fairly well established topography (Fretwell et al., 2013) and gravity anomaly (Scheinert et al., 2016) grids. However, the validity of the results derived from the spectral methods, particularly the Bouguer coherence, has been questioned where there is a lack of clear coherence between the topography and the gravity anomaly, which may be caused by the presence of buried loads (i.e. loads with no surface topographic manifestation) or the modification of topography by erosion (Kirby, 2014; McKenzie and Fairhead, 1997; Watts, 2001). It has been argued that the T_e estimates derived from the Bouguer coherence maybe consequently be biased towards high values, and should be considered upper bounds rather than best estimates (McKenzie and Fairhead, 1997). Moreover, in places of low RES coverage, Antarctic bed topography is often determined by inversion of gravity anomalies, which introduces circularity when T_e is estimated from the relationship *between* topography and gravity anomalies. These limitations mean that there is considerable uncertainty surrounding the use of inverse spectral methods to estimate T_e in Antarctica.

Fan wavelet techniques have recently been employed to determine variations in T_e across the entirety of Antarctica using the admittance and coherence methods (Chen et al., 2018; Ji et al., 2017). These methods show a strong contrast between predominantly high values in East Antarctica (T_e ~60–80 km) and low values in West Antarctica (T_e ~5–20 km) (Chen et al., 2018). However, the fan wavelet techniques also recover considerable variability within East Antarctica, with particularly high T_e values found in the Australian-Antarctic and Africa-Antarctic sectors, but relatively low values found in the Indian-Antarctic sector, including the Lambert Graben and Gamburtsev Subglacial Mountains (Figure 5c) (Chen et al., 2018).

Spatial patterns in Antarctic T_e recovered by both forward and inverse models tend to show broad first-order agreement, albeit from a limited set of results (Figure 5c). Significant uncertainty persists, however, as to the absolute values of T_e. The finding of a relatively weak West Antarctic lithosphere and a relatively rigid East Antarctic lithosphere may reflect the first-order differences between physical properties such as topography, crustal thickness, lithosphere thickness, lithosphere age, upper mantle viscosity, and heat flux in West and East Antarctica (An et al., 2015a, 2015b). The

differences in T_e *within* East Antarctica are indicative of spatial heterogeneities in the East Antarctic lithosphere, which may arise from the distinct thermotectonic histories of the different provinces (Chen et al., 2018). However, despite its importance in the context of long-term tectonic and topographic evolution, T_e in Antarctica remains poorly constrained.

2.3. Flexure and palaeotopography

2.3.1. Ice sheet loading

The most visible surface load in Antarctica today is the ice sheet itself (Figure 6). Isostatic models indicate that complete removal of the modern ice sheet load would result in up to 1 km of bedrock uplift, and an average increase in bedrock elevation of ~600 m (Paxman et al., 2019b). Any palaeotopography prior to Antarctic glaciation, or during a time at which the ice sheet was more restricted than today, was most likely characterised by higher average elevations. Under the modern ice sheet, ~45% of the bed currently situated beneath grounded ice is situated below sea level, whereas complete deglaciation would reduce this to ~19% (Paxman et al., 2019b). Ice sheet loading therefore has a significant effect on the extent of marine-based ice, which is most vulnerable to potential rapid retreat (see section 1.2). For an in-depth review of glacial isostatic adjustment on decadal to multi-millennial time scales, see Nield and Barletta (this volume).

2.3.2. Erosional unloading

Parts of the subglacial landscape of Antarctica have also been significantly modified by glacial erosion (Jamieson et al., 2005; Taylor et al., 2004). Removal of crustal mass by erosion ('erosional unloading') induces an isostatic response from the lithosphere, causing uplift of the remaining topography (Figure 6) (Molnar and England, 1990). Selective linear erosion, whereby basal melting and erosion are concentrated beneath thick ice in glacial troughs, while neighbouring peaks remain preserved beneath non-erosive ice (Sugden and John, 1976) and uplifted by the regional flexural adjustment to erosional unloading, is therefore optimal for creating substantial topographic relief.

Incision beneath major outlet glaciers dissecting mountain ranges around the Antarctic margin, such as the Beardmore and Byrd Glaciers in the Transantarctic Mountains (TAM) and the Recovery and Slessor Glaciers bounding the Shackleton Range, has produced subglacial troughs situated up to 3 km below sea level and differences in elevation between mountain peaks and trough floors of up to ~5 km over lateral distances of as little as 50 km (Fretwell et al., 2013; Morlighem et al., 2019). Elastic plate models show that the isostatic response to glacial incision can account for up to 2000 m of peak uplift in the central TAM and 1000 m in the Shackleton Range, which represents up to ~50% of the total peak elevations of the mountains (Paxman et al., 2017; Stern et al., 2005). In addition, flexural models, alongside geological observations such as uplifted fjordal sediments and detrital thermochronology, indicate that ~3 km of incision within the Lambert Graben (Thomson et al., 2013; Tochilin et al., 2012; White, 2013) has driven up to 1.4 km of post-Eocene flexural uplift along the graben flanks (Paxman et al., 2019b). In each of these examples, the high-amplitude flexural response is partly facilitated by relatively low regional T_e values (Figure 5), and has helped to generate as much as 4 km of additional topographic relief.

Many outlet glaciers across Antarctica appear to follow the underlying tectonic structure, such as the Lambert Glacier above the Mesozoic Lambert Graben (Ferraccioli et al., 2011). Pre-existing fault systems and associated topographic relief were likely first exploited by pre-glacial river systems (Jamieson et al., 2014; Sugden and Jamieson, 2018), and in turn by the early ice sheets, which progressively excavated the valleys to form deep subglacial troughs. Topographic steering became increasingly effective and ice flow and subglacial erosion became strongly focussed within the troughs, whereas removal of mass by erosion caused the adjacent highlands to be flexurally uplifted to elevations where relatively thin, non-erosive ice predominates, preserving the mountain peaks (Kessler et al., 2008; Paxman et al., 2017). Significant topographic relief can therefore be generated in Antarctica through a combination of (a) the relative efficacy of glacial erosion (Koppes and Montgomery, 2009), (b) peak preservation beneath non-erosive ice, and (c) flexural uplift induced by a relatively weak mantle lithosphere. Isostasy and lithospheric flexure can therefore drive and amplify feedbacks between tectonic structure, topography, climate and ice sheet behaviour.

Prior to glacial erosion and associated flexural uplift, the palaeotopography of Antarctica would have been characterised by considerably lower topographic relief, especially in the vicinity of the deep subglacial troughs near the coast, where fluvial valley networks could have only incised down to base level (Maritati et al., 2016; Paxman et al., 2017; Thomson et al., 2013; Wilson et al., 2012). The proportion of Antarctic topography situated below sea level ca. 34 Ma has been estimated at ~6%, compared to ~19% today (under ice-free conditions), with considerably less ice situated on deep, reverse-sloping beds (Paxman et al., 2019b). The overall effect of this change would be that earlier ice sheets were comparatively less susceptible to rapid, irreversible retreat associated with marine ice sheet instability processes. Prior to flexural uplift, the elevated terrain around the Antarctic margins would have been situated at lower average elevations at ca. 34 Ma, which could have influenced the timing and scale of early ice sheet nucleation. By contrast, the central highlands of East Antarctica, where long-term erosion rates are low (Cox et al., 2010; Jamieson et al., 2010; Jamieson and Sugden, 2008; Rose et al., 2013), and flexural responses to fluvial and alpine-style erosion are comparatively small (Paxman et al., 2016), have most likely remained relatively topographically stable over most of the past 34 Myr.

2.3.3. Mechanical unloading and thermal expansion

Lithospheric flexure can also occur in response to mechanical unloading and thermal expansion. Mechanical unloading takes place in extensional settings (e.g. rift systems) when slip on a normal fault causes unloading of the footwall block by removal of the hanging wall; the result is flexural isostatic rebound and uplift of the footwall rift flank (Figure 6) (Weissel and Karner, 1989). Thermal expansion (sometimes termed ‘thermal unloading’) occurs when the density of the lithosphere is reduced owing to lateral/vertical conduction of heat, which can induce a flexural response if the length of the thermal gradient does not exceed the flexural wavelength of the lithosphere (Figure 6). The TAM have been modelled as a flexurally-uplifted flank of the West Antarctic Rift System (WARS) arising from mechanical unloading on range-parallel normal faults bounding the WARS and thermal expansion due to lateral conduction of heat from higher-temperature mantle lithosphere beneath the WARS (see section 3.1) to lower-temperature mantle lithosphere beneath East Antarctica (Lawrence et al., 2006; Stern and ten Brink, 1989; ten Brink et al., 1997).

However, the TAM chain exhibits considerable variation in elevation and width along its length, which cannot be easily explained by uniform flexure along the mountain front (Olivetti et al., 2018; Paxman et al., 2019a). This variation may in part be explained by the presence of heterogeneous thermal anomalies within the upper mantle beneath the TAM front, which may provide spatially variable buoyant thermal loads (Brenn et al., 2017; Lawrence et al., 2006). Particularly problematic however are the southern TAM, where a high plateau extends for more than 300 km into East Antarctica (Fretwell et al., 2013). It is difficult to envisage how edge-driven flexure at the front of the TAM alone can account for such a broadly distributed, long-wavelength pattern of uplift, even for a highly rigid lithosphere (Paxman et al., 2019a) (see also section 4.2).

The significance of the location of the TAM along the tectonic boundary between West and East Antarctica has been noted by a number of authors (Brenn et al., 2017; Ebbing et al., 2018; ten Brink et al., 1997; van Wijk et al., 2008). This boundary likely had a bearing, at least in part, on the uplift of the TAM. Numerical models of lithospheric extension indicate that the inherited tectonic boundary between West Antarctica and cratonic East Antarctica focussed extensional deformation at the craton edge, resulting in a strongly asymmetric pattern of TAM uplift (van Wijk et al., 2008). Although the mechanism for TAM uplift remains debated (see section 4.2), the presence of an inherited tectonic boundary and the contrasting lithospheric properties of East and West Antarctica have likely played a significant role in the tectonic and topographic evolution of the TAM.

Inherited fault systems may also have played an important role in the topographic uplift of highlands such as the Shackleton Range and Gamburtsev Subglacial Mountains, where modelling studies indicate that mechanical unloading along border faults may have contributed up to 1 km of flexural uplift (Ferraccioli et al., 2011; Paxman et al., 2017). In the case of the Gamburtsevs, fault activity may be related to rifting within the Mesozoic East Antarctic Rift System (Ferraccioli et al., 2011), while fault activity in the Shackleton Range region may have most recently occurred in association with Weddell Sea rifting during the Cretaceous (Jordan et al., 2017; Krohne et al., 2016).

3. Thermal subsidence

Continental extension and rifting is a significant driver of surface topographic subsidence. During the 'syn-rift' phase, stretching and faulting are associated with thinning of the crust and lithosphere, which in turn leads to surface subsidence in order to retain isostatic equilibrium. The extent of crustal thinning is quantified by the stretching factor (β), which is defined as the ratio of original crustal thickness to final crustal thickness. Rifting is also associated with elevated lithospheric heat flux; in the 'post-rift' phase, following the cessation of extensional faulting, the decay of the thermal anomaly via heat conduction causes cooling and densification of the lithosphere, which in turn drives subsidence of the Earth's surface (McKenzie, 1978). Since lithospheric cooling is a transient process, thermal subsidence occurs over a protracted period of tens to hundreds of millions of years following a rifting event. It is therefore important to consider the effects of 'post-rift' thermal subsidence in the evolution of Antarctic palaeotopography since ca. 34 Ma.

3.1. West Antarctic Rift System

The West Antarctic Rift System (WARS) is believed to extend from the Ross Sea embayment through West Antarctica to the Bellingshausen Sea (Figure 7) (Bingham et al., 2012; Jordan et al., 2010;

LeMasurier et al., 1990; LeMasurier and Landis, 1996; Winberry and Anandakrishnan, 2004). The presence of an extensive rift system beneath the West Antarctic Ice Sheet (WAIS) is highly significant, because the low-lying topography (in places as deep as 2.5 km below sea level (Figure 7)) is hypothesised to render the WAIS vulnerable to rapid retreat due to marine ice sheet instability processes (Joughin and Alley, 2011; Mercer, 1978; Schoof, 2007; Thomas, 1979). Moreover, the bedrock geology and crustal structure of the rift system may influence the on-going and future dynamics of the overlying glaciers (Bingham et al., 2012; Rignot et al., 2008; Studinger et al., 2001), which in turn affect the stability of the wider ice sheet.

Rifting in West Antarctica is thought to have commenced at ca. 80–100 Ma (Siddoway et al., 2004), with the WARS subsequently experiencing 300–600 km of extension during the late Cretaceous and early Cenozoic (Behrendt et al., 1991; Cande et al., 2000; Wilson and Luyendyk, 2009). Consequences of this extension were the separation of Marie Byrd Land from East Antarctica and the opening of the Ross Sea basin (Decesari et al., 2007). Relative motion between East and West Antarctica was historically believed to have ended abruptly in the late Oligocene on the basis of marine magnetic anomalies from the northern Ross Sea (Cande et al., 2000). However, more recently acquired magnetic anomaly data indicate that motion between East and West Antarctica may have persisted up to the mid-Miocene (Granot and Dyment, 2018). Seismic and gravity data have recovered crustal thicknesses as low as 21 km beneath the WARS (An et al., 2015a; Jordan et al., 2010; Winberry and Anandakrishnan, 2004), indicating that the region has undergone significant crustal extension and thinning.

Rift-related magmatism appears to have commenced at ca. 48 Ma in the form of large alkaline plutons exposed in northern Victoria Land (Rocchi et al., 2002), where airborne magnetic data suggest similar intrusions may be extensive (Ferraccioli et al., 2009). By contrast, Cenozoic intrusive magmatism in Marie Byrd Land began at ca. 34 Ma (Rocchi et al., 2006). Effusive magmatism, in the form of Cenozoic volcanoes, has been documented in Victoria Land, Marie Byrd Land, and across the WARS (LeMasurier et al., 1990). Dating of edifices and associated deposits indicates that the earliest volcanism commenced at ca. 30 Ma, and a significant fraction of volcanic deposits date from after the mid-Miocene (ca. 14 Ma) (LeMasurier et al., 1990; LeMasurier and Landis, 1996; Rocchi et al., 2006; Shen et al., 2017; Stump et al., 1980). In addition to exposed magmatic rocks, aeromagnetic anomalies indicate that subglacial flood basalts may be preserved within the WARS (Behrendt et al., 1994). A recent inventory also indicates that there may be in excess of 138 subglacial volcanic cones across the WARS (van Wyk de Vries et al., 2018) (Figure 7), supporting the presence of an extensive and diffuse alkaline magmatic province (Finn et al., 2005).

An implication of the thermotectonic history of the WARS is that the palaeotopography of West Antarctica was considerably higher prior to and during late Cretaceous and Cenozoic crustal extension and heating than at the present-day. This interpretation is supported by the presence of flat bedrock platforms of proposed Miocene age currently situated below sea level in the Ross Sea Embayment (Figure 7) (Wilson and Luyendyk, 2006). These plateaus are interpreted as having formed by wave erosion at sea level, yet are currently situated at water depths ranging from ~150 to ~350 m below sea level, deepening southwards towards the TAM (Wilson and Luyendyk, 2006). These observations imply regional subsidence of the Ross Sea Embayment since the Neogene, with a combination of younger and/or higher magnitude extension towards the TAM. In addition, coring at

Deep Sea Drilling Project (DSDP) Site 270 in the Ross Sea (Figure 7) recovered a terrestrial palaeosol several metres deep developed on a sedimentary breccia above basement gneiss at ~1000 m below sea level (Ford and Barrett, 1975). The palaeosol is overlain by quartz sand and glauconitic greensand, which are dated at ca. 26±1.5 Ma and interpreted as having been deposited in a near-shore or shallow marine environment (Barrett, 1975; De Santis et al., 1999; Kulhanek et al., 2019). This stratigraphy is consistent with a marine transgression and implies a significant amount of regional subsidence since the early Oligocene.

The first attempt to produce a model of post-Eocene thermal subsidence in the WARS assumed that the rift system comprises five non-overlapping regions, each representing a different phase of the regional extension history (Wilson and Luyendyk, 2009). Each phase was assumed to have a uniform stretching factor and an instantaneous age of extension, permitting the use of a simple 1D cooling model (McKenzie, 1978) to predict the amount of post-34 Ma thermal subsidence across the WARS. The amount of thermal subsidence (S) as a function of time (t) is given by (McKenzie, 1978)

$$S(t) = \frac{4a\rho_m \alpha T_m}{\pi^2(\rho_m - \rho_i)} \frac{\beta}{\pi} \sin\left(\frac{\pi}{\beta}\right)\left(1 - e^{-t/\tau}\right) \quad (3)$$

where

$$\tau = \frac{a^2}{\pi^2 \kappa} \quad (4)$$

where a is the thickness of the lithosphere, α is the coefficient of thermal expansion, T_m is the temperature at the base of the lithosphere, κ is the thermal diffusivity of the lithosphere, ρ_m is the density of the lithospheric mantle, ρ_i is the density of the material infilling the surface subsidence, β is the stretching factor, and τ is thermal decay time constant.

For their five phases of extension in the WARS, Wilson and Luyendyk (2009) used β factors from 2 to 6 and mean extension ages of 93 to 38 Ma (moving southwest from Marie Byrd Land towards the TAM; Figure 8). This model, with the locus of extension progressively shifting towards the TAM, predicts ~500 m of post-34 Ma subsidence in the central WARS (Figure 8) (Wilson and Luyendyk, 2009). The above rifting parameters were constrained by the necessity to restore the terrestrial palaeosol at DSDP Site 270 to sea level at ca. 34 Ma, which required that extension in the central Ross Sea is younger than 70 Ma with a stretching factor of >2.0 (Wilson et al., 2012; Wilson and Luyendyk, 2009). By correcting for thermal subsidence (following Wilson and Luyendyk, 2009), erosion, flooding of the subsided area with water, and associated flexural isostatic responses, the reconstruction process of Wilson et al. (2012) produced a substantial upland feature in West Antarctica, with elevations of 500–1000 m above sea level. The stretching factors also implied a pre-extension crustal thickness of ~50 km in the WARS (Wilson and Luyendyk, 2009). These results could be interpreted as lending to support to the suggestion that a significant highland plateau and thickened crust existed in West Antarctica prior to extension, of which the Transantarctic Mountains are a remnant (Bialas et al., 2007; Huerta, 2007). Terrestrial and marine microfossil assemblages obtained via sub-ice drilling near the Siple Coast are indicative of low-elevation coastal plain and shallow marine palaeoenvironments during the Eocene (Coenen et al., 2019). This finding

contradicts the presence of a uniformly high Siple Coast region during the Eocene (Wilson et al., 2012); an alternative scenario is that the palaeotopography was characterised by greater relief, with low-lying areas in the regions now occupied by ice streams and higher terrain in between.

A more recent reconstruction of Antarctic palaeotopography at the Eocene–Oligocene boundary topography (Paxman et al., 2019b) produced palaeo-elevations for the WARS up to 500 m lower than that of Wilson et al. (2012). This difference arises from a combination of updated observed offshore sediment volumes and modelled onshore erosion patterns, as well as updated constraints on the modern regional bedrock topography and T_e. Use of a simple 1D exponential decay model (McKenzie, 1978) to compute the temporal history of thermal subsidence since ca. 34 Ma (Equation 3; Figure 8), predicted that DSDP Site 270 subsided below sea level at ca. 28 Ma (Paxman et al., 2019b), in good agreement with the recorded drill core stratigraphy (Kulhanek et al., 2019; Leckie and Webb, 1983).

Since many subglacial volcanoes across the WARS may have been emplaced since ca. 34 Ma, these edifices were removed from the recently updated ca. 34 Ma palaeotopography (Paxman et al., 2019b). The approximate geometry of each volcanic edifice was determined using a recent inventory of the distribution, height, and diameter of subglacial volcanic cones across West Antarctica (Figure 8) (van Wyk de Vries et al., 2018), and these cones were then subtracted from the palaeotopography (Paxman et al., 2019b). Since the average diameter of these volcanic cones is 21 km, which is smaller than the flexural length scale of the lithosphere, no flexural isostatic adjustment is required when they are removed from the topography. Moreover, any influence of the edifices (or lack thereof) on past ice sheet dynamics would be highly localised, and largely insignificant within continental-scale ice sheet models with spatial resolutions of >10 km.

3.2. Passive continental margins of East Antarctica

The transient effects of thermal subsidence are not solely pertinent to West Antarctica. During the early Mesozoic, East Antarctica was part of the supercontinent of Gondwana, and was situated in the centre of landmasses that constitute modern-day South America, Africa, Madagascar, India, and Australia. Gondwana break-up began in the Jurassic ca. 180–160 Myr ago (Dalziel, 1997) with the separation and movement northwards of South America and Africa away from East Antarctica. Break-up then proceeded clockwise around East Antarctica with the successive separation of India and then Australia (Boger, 2011 and references therein). East Antarctica is now bounded by passive margins (Sugden and Jamieson, 2018), which are separated from their conjugates in southern Africa, eastern India, and southern Australia by oceanic spreading ridges. These continents each contain Jurassic basalts and dolerite sills formed during volcanic activity associated with the break-up of Gondwana. In Antarctica, these rocks form the Ferrar Large Igneous Province (Elliot and Fleming, 2004).

The East Antarctic passive margins would have experienced post-rift thermal subsidence, causing the continental shelves to subside and providing additional accommodation space for sediments being delivered to the continental margin via erosion and transport by ice or rivers (Jamieson et al., 2008, 2005). The break-up age of each sector of the Antarctic margin is well constrained from the age of the oldest sea floor (Müller et al., 2016), although the stretching factor and initial timing of

continental rifting are more difficult to evaluate. A recent attempt to restore Antarctic margin palaeotopography (since ca. 34 Ma) for the effects of residual post-rift cooling (Paxman et al., 2019b) adopted a 1D cooling model (McKenzie, 1978) (Equation 3) using the observed age of the sea floor (Müller et al., 2016) and a uniform β value of 4 across the widths of the continent-ocean transitions around Antarctica (Gohl, 2008). The modelled magnitude of post-Eocene thermal subsidence around the margins of East Antarctica varies from ~300 m for the earliest-formed continental shelves (e.g. offshore Dronning Maud Land), where separation occurred in the Jurassic, to up to ~1200 m for the shelves that experienced separation as recently as the late Cretaceous (e.g. offshore George V Land) (Paxman et al., 2019b). However, no firm geological constraints that provide a record of post-Eocene thermal subsidence around the margin of East Antarctica have yet been documented.

4. Dynamic topography

Dynamic topography is a collective expression for changes in Earth's surface elevation caused by vertical tractions exerted on the base of the lithosphere by the convecting sub-lithospheric (viscous) mantle (Flament et al., 2013; Hager et al., 1985; Molnar et al., 2015; Pekeris, 1935). Convective flow within the mantle is driven by the buoyancy effects of density anomalies, which are in turn caused by variations in temperature and/or composition. When this viscous flow interacts with the surface boundary, viscous normal stresses are generated, causing vertical deflection of the surface. Upward flow towards the surface leads to positive dynamic topography (surface uplift), whereas downward flow away from the surface leads to negative dynamic topography (surface subsidence) (Braun, 2010).

Surface manifestations of dynamic topography can range from distributed long-wavelength continental tilting (Quigley et al., 2010; Richards et al., 2016; Sandiford et al., 2009), to more focussed surface uplift above the impingement of a mantle plume on the base of the lithosphere (Behrendt et al., 1991) or subsidence above a subducting lithospheric slab (Whittaker et al., 2010). Ocean floor residual depth measurements from the Southern Ocean reveal dynamic topography amplitudes of up to 1 km and wavelengths of 10^3–10^4 km, with spatial variability in magnitude and direction (Hoggard et al., 2017, 2016). The temporal pattern of dynamic uplift/subsidence is typically derived from marine stratigraphy, with evidence for typical peak rates on the order of 100 m/Myr (Al-Hajri et al., 2009; Czarnota et al., 2013; Japsen et al., 2006; Richards et al., 2016). This implies that long-wavelength changes in bedrock elevation in Antarctica over multi-million year timescales may be attributed, at least in part, to changes in dynamic topography.

4.1. Marie Byrd Land

Marie Byrd Land is defined by a 1000 x 500 km dome-shaped volcanic province (Figure 7) comprising a series of large shield volcanoes and an extensive sequence of alkali basalts up to ca. 28–30 Ma in age (LeMasurier et al., 1990; Rocchi et al., 2006). The geochemistry of basalts in Marie Byrd Land and the WARS is comparable to those found on oceanic islands associated with well-established hot spot tracks (e.g. Hawaii) (Hole and LeMasurier, 1994; LeMasurier and Rex, 1989), supporting the suggestion of a mantle plume beneath the WARS (Behrendt et al., 1991) (see also Bredow and Steinberger, this volume). In addition, several low-relief surfaces at scattered localities across Marie

Byrd Land with elevations up to 2.7 km have been interpreted as remnants of a continuous, low-relief surface (LeMasurier and Landis, 1996). It has been proposed that this erosion surface formed close to base level, and has been uplifted by up to ~2.7 km since ca. 28–30 Ma, accompanied by block faulting and alkali basalt volcanism, all of which may signal the impingement of a mantle plume on the base of the West Antarctic lithosphere (LeMasurier and Landis, 1996).

However, the suggestion of a mantle plume beneath the WARS is controversial; the volume of magmatism imaged within the WARS by geophysical data implies time-averaged magma production rates much lower than those expected for a mantle plume-dominated setting, especially one with relatively thin lithosphere (Rocchi et al., 2002). Recent attempts to resolve this controversy have centred on the development of new seismic tomography models for the upper mantle beneath West Antarctica (An et al., 2015b; Lloyd et al., 2015; Shen et al., 2018; Bredow and Steinberger, this volume; Wiens et al., this volume). An approximately circular P- and S-wave low-velocity anomaly in the upper mantle would be indicative of a warm thermal anomaly, potentially related to a mantle plume. Such an anomaly is not clearly visible beneath central West Antarctica (An et al., 2015a), but may be resolved beneath Marie Byrd Land, although its depth extent is poorly constrained (Figure 9) (Lloyd et al., 2020, 2015; Shen et al., 2018). Seismic wave velocities and receiver functions show that the crust beneath the high topography in Marie Byrd Land is up to 10 km thicker than beneath the WARS, indicating that this high topography is at least partially supported isostatically rather than entirely dynamically by a mantle plume (Shen et al., 2018). However, satellite gravity gradients show a bowl-shaped structure in Marie Byrd Land, possibly originating from a mantle plume source (Ebbing et al., 2018; Pappa and Ebbing, this volume).

It is therefore possible, but not conclusively demonstrated, that the long-wavelength, high-elevation domal topography of Marie Byrd Land, anomalous when compared to the adjacent WARS, is in part supported by a hotspot-related thermal anomaly within the upper mantle. If this is the case, understanding the plume-induced topographic evolution of Marie Byrd Land is important for attempts to reconstruct regional palaeotopography. The beginning of Marie Byrd Land uplift was initially assumed to have been contemporaneous with early Oligocene magmatism (ca. 28–30 Ma) (LeMasurier and Landis, 1996), although older volcanic units may have been emplaced but subsequently eroded or not yet sampled. It is possible that dynamic uplift commenced earlier, in response to mantle upwelling during the Cretaceous and early Cenozoic after cessation of subduction following Gondwana break-up (Sutherland et al., 2010). Conversely, recent apatite fission track and (U–Th–Sm)/He thermochronology data have been used to tentatively suggest that denudation (and associated uplift) in Marie Byrd Land commenced in the early Miocene (ca. 20 Ma) (Spiegel et al., 2016). However, most low-temperature cooling ages from Marie Byrd Land date to 100–60 Ma, and the 20 Ma age group is based on only two rock samples from one location ~250 km from the centre of the dome (Spiegel et al., 2016). Consequently, the questions of whether Marie Byrd Land was uplifted due to mantle plume activity, and the magnitude and timing of any dynamic uplift, remain matters of considerable uncertainty.

Large-scale continental glaciation in coastal West Antarctica would require areas of land situated at significant elevations above sea level. Marie Byrd Land is therefore a potential candidate for ice sheet inception in West Antarctica. Ice sheet model simulations performed on the palaeotopographic reconstructions of Wilson et al. (2012) suggest that the high palaeo-elevations in

Marie Byrd Land and central West Antarctica could have permitted the establishment of a significant WAIS at ca. 34 Ma (Wilson et al., 2013). Significant ice still accumulates in the minimum ca. 34 Ma palaeotopography of Wilson et al. (2012), which includes a correction for 1 km of post-34 Ma dynamic uplift in Marie Byrd Land. However, if uplift of up to 2.7 km (LeMasurier and Landis, 1996) commenced at ca. 20 Ma (Spiegel et al., 2016), Marie Byrd Land would have been low-lying at ca. 34 Ma, and regional ice sheet inception may have occurred during the early Miocene at the earliest. This is turn presents a dilemma as to whether/where ice accumulated in West Antarctica during the early Oligocene, which has implications for global ice volumes, sea level and ocean temperature at this time (Wilson et al., 2013)Since the magnitude of post-Eocene dynamic uplift across Marie Byrd Land may have been anywhere between 0 and 2.7 km, a high degree of uncertainty persists in our understanding of the topographic evolution and glacial history of Marie Byrd Land.

This case study highlights the potential importance of sub-plate processes such as the vertical tractions imposed on the base of the lithosphere by buoyant mantle plumes for the evolution of Antarctic palaeotopography, and in turn for Antarctic glacial history. As well as influencing past ice sheet dynamics via changes in topography, the presence of a mantle plume beneath Marie Byrd Land may also elevate the local geothermal heat flux to values of up to 150 mW/m^2 (Seroussi et al., 2017), and in turn increase the rate of basal melting beneath the ice sheet, with consequences for ice sheet hydrology (Seroussi et al., 2017).

4.2. Transantarctic Mountains

As outlined in section 2.3, the origin of the Transantarctic Mountains (TAM) remains a major open question in the history of Antarctica's subglacial topography. Some studies have proposed that the TAM are isostatically supported by a thickened crust, with gravity modelling implying crustal thicknesses ~5–10 km greater than those beneath the Wilkes Subglacial Basin in the immediate hinterland (Jordan et al., 2013; Studinger et al., 2004). However, although recent seismic studies find a modest (~5 km) crustal root beneath the TAM, it does not appear to fully support the observed topography (An et al., 2015a; Chaput et al., 2014; Hansen et al., 2016; Lawrence et al., 2006; Ramirez et al., 2016). The absence of a fully compensating crustal root is more consistent with a flexural origin for the TAM. However, as discussed in section 2.3.3, a problematic observation for the flexure model is that the southern TAM are particularly broad, with a high plateau extending for more than 300 km into East Antarctica (Fretwell et al., 2013), which is inconsistent with solely edge-driven flexure at the front of the TAM.

Recently constructed seismic tomographic images of the uppermost mantle beneath the southern TAM reveal a potential mantle source of the observed broad topographic plateau (Shen et al., 2017; Wiens et al., this volume). Seismically slow uppermost mantle beneath the southern TAM (Figure 9) is indicative of a hot temperature anomaly capable of reducing the upper mantle density by ~1–1.5%, which would provide sufficient buoyancy to support ~1.5–2.0 km of surface elevation (Shen et al., 2017). Tomography images also reveal a fast seismic anomaly beneath the slow uppermost mantle (Figure 9), which is interpreted as foundering lithosphere that is being replaced at shallow depths by a warmer, wedge-shaped body of asthenosphere (Shen et al., 2018, 2017). Cretaceous–Cenozoic rifting within the WARS may have caused thermal destabilisation and ultimately delamination of pre-existing cold lithospheric mantle, thereby triggering lithospheric foundering

(Shen et al., 2017). Better understanding of the timing of lithospheric foundering and buoyant uplift of the southern TAM plateau is required for more accurate reconstructions of the regional palaeotopography.

4.3. Wilkes Subglacial Basin

The Wilkes Subglacial Basin (WSB) is situated in the immediate hinterland of the TAM (Figure 2). As a low-lying marine basin containing an ice volume equivalent to ~5 metres of global sea level rise (Fretwell et al., 2013; Gasson et al., 2015), an understanding of ice sheet behaviour within the WSB during past warmer climates is of particular importance for predicting future ice sheet change in this sector of the East Antarctic Ice Sheet (EAIS). However, significant variation remains between numerical ice sheet model predictions of EAIS retreat within the WSB during past warm periods such as the mid-Pliocene (ca. 3 Ma) (DeConto and Pollard, 2016; Mengel and Levermann, 2014; Pollard and DeConto, 2009), at which time atmospheric CO_2 levels were similar to that of today (~400 ppm). Improved understanding of past ice sheet dynamics within the WSB relies in part on understanding the evolution of the subglacial topography of the basin (Paxman et al., 2018).

Austermann et al. (2015) used the 'ASPECT' mantle convection code (Bredow and Steinberger, this volume) to model changes in dynamic topography in the WSB since the mid-Pliocene (Figure 10). The present-day dynamic topography field was computed from the modern density and viscosity structure of the mantle (as constrained from seismic tomography and mineral physics). Changes in local dynamic topography were assumed to arise entirely from the motion of the Antarctic plate through this dynamic topography field (Austermann et al., 2015). This combined mantle flow and plate motion modelling approach predicted that the bed of the northern WSB (close to the present-day ice margin) was ~100–200 m lower during the mid-Pliocene than today (Figure 10) (Austermann et al., 2015). Incorporating this change in bed elevation into an ice sheet model (Pollard and DeConto, 2009) resulted in an additional 200–560 km of grounding line retreat into the WSB under a mid-Pliocene climate (Figure 10) (Austermann et al., 2015). The implication is that a relatively modest amount of dynamic uplift of the WSB since 3 Ma has acted to significantly increase the stability of this sector of the EAIS.

Austermann et al. (2015) also computed the change in dynamic topography across the entirety of Antarctica since 3 Ma (Figure 10), and found that the amplitude of dynamic topography change in other marine-based sectors of the EAIS such as the Aurora or Recovery subglacial basins was relatively small by comparison to the WSB, with little impact on ice sheet behaviour. This study calculates the mantle flow field from the present-day density and viscosity structure of the mantle. Constraining these parameters – and the mantle flow field – in the geological past is particularly challenging, especially in Antarctica, and results in large uncertainties in predictions of changes in dynamic topography over multi-million year timescales. Moreover, numerical mantle convection models tend to over-predict the amplitudes of dynamic topography measured from (e.g.) residual depth anomalies in the oceanic realm (Hoggard et al., 2016), indicating that mantle flow models alone cannot yet be relied upon to reliably correct for dynamic topography changes.

4.4. Antarctic-wide dynamic topography

Aside from the use of mantle flow simulations, separate attempts have been made to constrain continental-scale patterns of dynamic topography in Antarctica using geophysical datasets. For example, the seismic crustal thickness can be used to calculate surface elevations that would result if topography were entirely supported by variations in crustal thickness (Airy isostasy; section 2.1).

$$h_{isostatic} = \frac{(\rho_m - \rho_c)}{\rho_m}(T_c - T_0) \quad (5)$$

where T_c is the observed crustal thickness, T_0 is the zero-elevation crustal thickness, ρ_m is the density of the mantle, ρ_c is the density of the crust, and $h_{isostatic}$ is the 'isostatic topography' – that is, the topography supported by isostatic buoyancy forces. The isostatic topography can be subtracted from the observed topography to give a 'residual topography', which may be, to some extent, supported by vertical tractions applied to the base of the lithosphere by the convecting mantle (Cazenave et al., 1989; Forte et al., 1993; Menard, 1973; Molnar et al., 2015).

Comparison of Antarctica's observed bedrock topography (Fretwell et al., 2013) with the computed isostatic topography indicates that local crustal thickening beneath the highlands of the Gamburtsev Subglacial Mountains and Dronning Maud Land can support their differential elevation above the broader East Antarctic plateau (Figure 11) (O'Donnell and Nyblade, 2014). However, the modal elevations of the plateau itself are ~700 m higher than can be accounted for based on its crustal thickness relative to that of the rest of East Antarctica (Figure 11) (O'Donnell and Nyblade, 2014). This Airy isostatic deficit beneath the East Antarctic plateau is also noted from Moho depths derived from gravity inversions (Pappa et al., 2019; Pappa and Ebbing, this volume). Both studies speculate that this anomalous topography may be supported by a mid-to-lower mantle source, and is therefore 'dynamic' (O'Donnell and Nyblade, 2014; Pappa et al., 2019).

However, calculations attempting to separate isostatic and dynamic topography are subject to a number of uncertainties:

1. Isostatic topography is calculated assuming an Airy model of isostasy, and so does not account for elastic plate flexure (see section 2.1).
2. Crustal thickness observations are often unreliable or associated with large uncertainties. In Antarctica, crustal thickness is either estimated from satellite gravity inversion models (Block et al., 2009; Pappa et al., 2019; Pappa and Ebbing, this volume) or from seismic receiver functions (An et al., 2015a; Hansen et al., 2010; Wiens et al., this volume), which are typically associated with uncertainties of at least ±4 km, which translate into uncertainties of ±~700 m in the isostatic topography.
3. The density contrast between the lower crust and the lithospheric mantle is often also associated with large uncertainty.

Gravity anomalies, rather than crustal thickness measurements, are considered by several authors to offer the tightest constraints on dynamic topography in the continents (McKenzie, 2010; Molnar et al., 2015). Numerical models of convective mantle flow indicate that the expected ratio between the 'dynamic' free-air anomaly and topography (the 'convective admittance') is ~30 mGal/km for

water/ice-covered terrain (McKenzie, 1994; McKenzie et al., 1974). This 'rule' for converting free-air anomalies into dynamically supported topography is generally supported by limited observations in the oceanic realm (Hoggard et al., 2017; Winterbourne et al., 2014). The long-wavelength gravity field (>3300 km (Watts and Moore, 2017)) can therefore be scaled using the convective admittance to produce an estimate of dynamic topography (Figure 11) (Hoggard et al., 2017, 2016).

However, this approach has not so far been used for Antarctica, and there are reasons to exercise caution with its application. Recent models of mantle convection show that the sensitivity kernels for gravity and topography are different, such that the relationship between 'dynamic' gravity and topography is not summarised by a constant admittance, but one which is a function of the wavelength and depth of the driving buoyancy anomaly (Colli et al., 2016). Sizeable dynamic topography may therefore exist without a corresponding gravity anomaly, and vice versa. Indeed, the correlation between residual topography (from crustal thickness measurements) and dynamic gravity is generally poor (Figure 11).

The spatial and temporal evolution of the amplitude and direction of changes in dynamic topography in Antarctica since ca. 34 Ma remain poorly understood. Development of an Antarctic palaeo-dynamic topography model will require an expanded coverage of seismic stations in Antarctica, and a reduction in the epistemic uncertainty within mantle flow models. Also required is the identification of readily dated geological markers that can constrain the magnitude and pattern of dynamic uplift or subsidence on length scales of 100s to 1000s of km, although such exposure does not exist in Antarctica. These limitations and uncertainties become increasingly problematic when moving further back in time, which makes reconstructing changes in dynamic topography over the course of Antarctica's glacial history (since ca. 34 Ma) particularly challenging.

5. Conclusions

The preceding sections have illustrated the influences of the Antarctic mantle on palaeotopography. Section 2 illustrated how lithospheric flexure has acted to increase (ice-free) bed elevations in regions subjected to unloading of the lithosphere via glacial erosion, extensional faulting, and conduction of heat within the lithosphere (Figure 6). Section 3 highlighted the role of protracted lithospheric cooling in Antarctica, primarily in the West Antarctic Rift System. The result has been gradual topographic subsidence of up to 1 km since ca. 34 Ma (Figure 8) (Wilson and Luyendyk, 2009). Section 4 showed that it remains difficult to evaluate long-term changes in mantle convection and dynamic topography over geological timescales in Antarctica, despite recent modelling results from the Wilkes Subglacial Basin (Figure 10) (Austermann et al., 2015).

The nature of the Antarctic mantle, and its role in the evolution of subglacial topography, has a number of implications for the past behaviour of the AIS.

1. Early Antarctic ice sheets likely exploited pre-existing tectonic structures such as fault systems and their associated topography. Subsequent excavation of deep subglacial troughs and associated flexural uplift of the trough flanks facilitated effective focussing of glacial flow and erosion within the troughs and contemporaneous preservation of the adjacent highlands beneath non-erosive ice. The patterns of

glacial erosion and flexural uplift are therefore governed in part by pre-existing structural weaknesses within, and the flexural rigidity of, the Antarctic lithosphere.

2. Reconstructions of palaeotopography at ca. 34 Ma have significantly less area below sea level and much shallower marine basins than the modern topography (Paxman et al., 2019b; Wilson et al., 2012). This is largely due to bed overdeepening by glacial erosion (see above), and subsidence driven by post-rift lithospheric cooling. Widespread subsidence of up to 1 km in West Antarctica (Wilson et al., 2012; Wilson and Luyendyk, 2009) has resulted in the development of an extensive area of low-lying, reverse-sloping topography beneath the WAIS. Landscape evolution models indicate that much of West Antarctica had subsided below sea level by the mid-Miocene (ca. 14 Ma) (Paxman et al., 2019b). The WAIS may therefore have become increasingly sensitive to marine ice sheet instability processes and associated rapid and irreversible losses of ice volume after this time. Moreover, the presence of higher palaeotopography in West Antarctica could have facilitated the nucleation of a considerable palaeo-WAIS in the early Oligocene (Wilson et al., 2013).
3. Changes in dynamic topography of as little as 100–200 m have potentially induced significant changes in ice sheet sensitivity in the Wilkes Subglacial Basin since as recently as the mid-Pliocene (ca. 3 Ma) (Austermann et al., 2015). Considerable uncertainty remains, however, regarding the spatial and temporal evolution of Antarctic dynamic topography through the Cenozoic, with potentially major ramifications for ice sheet stability and sea level change.

Overall, palaeotopographic reconstructions and ice sheet models suggest that the evolution of the subglacial topography of Antarctica has important implications for past Antarctic ice sheet behaviour (and in turn global sea levels), in terms of the extent and rate of (i) ice growth during cold climate intervals, and (ii) ice loss during warm climate intervals (Colleoni et al., 2018; Gasson et al., 2016; Wilson et al., 2013). This modification of the subglacial landscape and associated impact on ice sheet behaviour can be attributed to interactions and feedbacks between surface, crustal, and mantle processes, such as glacial erosion, faulting, flexure, thermal subsidence, and dynamic topography. An improved understanding of mantle properties and processes, including in particular (a) a more robust model of the flexural rigidity of Antarctica's lithosphere, (b) further constraints on the pattern of thermal subsidence in West Antarctica and around the margins of East Antarctica, and (c) a better understanding of changes in mantle convection patterns and associated changes dynamic topography, on the evolution of Antarctic palaeotopography is therefore a key priority in the next generation of Antarctic landscape evolution and ice sheet models.

Acknowledgements

The author would like to acknowledge the support of a Natural Environment Research Council UK studentship (NE/L002590/1). Many of the topics described in this chapter are based on contributions

from the ANTscape working group within the Past Antarctic Ice Sheet dynamics (PAIS) research programme of the Scientific Committee on Antarctic Research (SCAR). I would like to acknowledge the support of the major contributors to this programme, including Peter Barrett, Graeme Eagles, Karsten Gohl, Katharina Hochmuth, Stewart Jamieson, German Leitchenkov, Doug Wilson, and the numerous attendees of the various ANTscape workshops on Antarctic palaeotopography and palaeobathymetry that were instrumental in the development of several concepts reviewed in this chapter. I would also like to extend thanks to Mark Hoggard and Doug Wilson for their thorough and constructive reviews, which greatly improved the quality of this chapter.

Figure captions

Figure 1. Measurement of ice thickness and subglacial topography using radio-echo sounding (RES). (a) Schematic of an airborne RES survey. The aircraft emits a series of radar pulses (red dashed lines), which are reflected at interfaces including the ice surface, internal layers within the ice sheet, and the ice-bed interface. The amount of radar energy reflected depends on the acoustic impedance contrast at the interface. The aircraft then receives the return echoes, and their travel time is used to calculate the depth to the reflector. (b) Coverage of RES measurements in Antarctica. Red lines denote surveys that were included in the Bedmap2 compilation (Fretwell et al., 2013); blue lines denote more recently acquired survey data (Forsberg et al., 2018; Humbert et al., 2018; Jordan et al., 2018; Karlsson et al., 2018; Tinto et al., 2019). (c) Example of a radar trace (echogram) from Antarctica (Leuschen et al., 2016). Elevations are relative to the WGS84 ellipsoid. The y-axis is converted from time to depth assuming a radar velocity in ice of 168 m/μs. Reflectors from the ice surface and ice sheet bed are clearly visible, as are faint internal layer reflections within the ice sheet.

Figure 2. Bed topography of Antarctica. Bed elevations and bathymetry are from the Bedmap2 dataset (Fretwell et al., 2013). Elevations are in metres above mean sea level (m.a.s.l.) and contoured at 1000 m intervals. Major geographical and topographical features are labelled. The dark lines around the edge of the continent denote the modern grounding line and ice shelf calving front. Approximately 45% of the bed is presently situated below sea level, including the extensive Recovery, Wilkes and Aurora subglacial basins in East Antarctica, wherein the deepest regions are ~2 km below sea level (Fretwell et al., 2013).

Figure 3. Cenozoic ice sheet and climate history of Antarctica (modifed from Zachos et al. 2008, with permission from Springer Nature, ©2008). Curve shows the Cenozoic stacked benthic foraminifera oxygen isotope record, based on deep-sea sediments obtained at Deep Sea Drilling Project and Ocean Drilling Program sites (Zachos et al., 2001, 2008). The raw data have been smoothed using a five-point running mean. $\delta^{18}O$ isotope values are given in parts per thousand (‰). The temperature scale is calculated for ice-free conditions, so only applies to the time interval preceding glaciation in Antarctica. The greenhouse-icehouse transition and the formation of large-scale ice sheets on Antarctica coincides with the step increase in $\delta^{18}O$ at the Eocene–Oligocene boundary (ca. 34 Ma). The approximate ice extents for different stages (shaded black) are derived from ice sheet modelling (Jamieson et al., 2010). The Oligocene to middle Miocene witnessed numerous glacial cycles, with the ice sheet waxing and waning in concert with orbital cycles. Subsequent Miocene cooling allowed the ice sheet to advance to the continental shelf edge, perhaps on multiple occasions. Abbreviations: Cret. = Cretaceous; Plio. = Pliocene; Plt. = Pleistocene.

Figure 4. Schematic summary of the interactions between mantle processes and topography beneath ice sheets. Changes in surface loading due to (e.g.) erosion or ice margin retreat induce a flexural isostatic response within the elastic lithosphere. Topographic subsidence occurs in response to lithospheric stretching and subsequent 'post-rift' cooling, re-thickening and densification, and commonly allows sediments to accumulate in the resulting basin. Deposition of sediments in turn triggers a flexural isostatic response, causing further subsidence. Heating of the lithosphere can induce partial melting, which leads to subglacial volcanism. Heating can also induce topographic uplift, as can normal tractions imparted on the base of the lithosphere by the convecting viscous mantle (dynamic topography).

Figure 5. Effective elastic thickness estimation in Antarctica. (a) Forward modelling of flexed topography along a profile crossing the Bailey Ice Stream and Theron Mountains, East Antarctica (modified from Paxman et al., 2017). Elastic plate models (black lines) indicate that the observed topography (red line) is best fit with a T_e value of 25 km. (b) Inverse (spectral) modelling of topography and gravity anomaly data for the region of East Antarctica including the profile in panel a. Comparison of the calculated free-air admittance (red circles with standard error bars) with model curves recovers a best fitting T_e of 18 km (modified from Paxman et al., 2017). (c) T_e map for Antarctica derived using a fan wavelet method to compute the Bouguer coherence (Chen et al., 2018). Coloured shapes denote published regional T_e estimates using forward (diamonds) and inverse (circles) modelling.

Figure 6. Causes of lithospheric flexure in Antarctica. Diagrams are schematic, although representative horizontal and vertical scales are provided. (a) Ice loading, causing the land to be depressed beneath an ice mass, such as the AIS. Peripheral bulges are uplifted around the margin of the ice sheet. (b) Erosional unloading, caused by excavation of material by rivers or glaciers. The flexed topography exhibits uplifted flanks dipping gently away from the valley. Such topography is observed around numerous large outlet glaciers in Antarctica, such as the Lambert Glacier (White, 2013). (c) Mechanical unloading, caused by shear along a normal fault plane. The footwall block is unloaded and flexurally uplifted, whereas in the hangingwall block surface material is replaced by mantle, causing loading and flexural subsidence (Weissel and Karner, 1989). Such topography is observed along the flanks of major extensional fault systems, such as in the Shackleton Range (Paxman et al., 2017). (d) Thermal expansion (/ 'unloading'), caused by horizontal heat conduction within the lithosphere. Heat is conducted from areas of high temperature to areas of low temperature, and modifies the thermal buoyancy of the lithosphere, which induces a flexural response if the length of the thermal gradient ≤ the flexural wavelength of the lithosphere (λ). This process has been hypothesised to partially explain the uplift of the Transantarctic Mountains (TAM) (Brenn et al., 2017; Stern and ten Brink, 1989; ten Brink et al., 1997).

Figure 7. West Antarctic Rift System. Present-day bed elevations are shown relative to mean sea level (Paxman et al., 2019b). Contour interval is 1 km. Dashed magenta lines show the extent of the West Antarctic Rift System. An explanation of the symbology is provided in the figure legend. Red circles denoting volcanic edifices are proportional (4x true scale) to the basal diameter of the cone (van Wyk de Vries et al., 2018). Subglacial trenches and rift valleys (black outlines), as well as submerged flat-topped bedrock platforms (blue polygons) are imaged by radar and gravity/magnetic anomaly data (Bell et al., 1998; Bingham et al., 2012; Studinger et al., 2001; Wilson and Luyendyk, 2006).

Figure 8. Thermal subsidence in West Antarctica (modified from Paxman et al., 2019b). (a) Magnitude of post-34 Ma thermal subsidence associated with the West Antarctic Rift System (Wilson et al., 2012; Wilson and Luyendyk, 2009). Dashed white lines mark modelled areas of uniform stretching factor (β) corresponding to five phases of extension in the WARS (Wilson and Luyendyk, 2009). The inset table lists the β value and mean age of extension associated with each phase. Filled red circles denote volcanic edifices; circle size is proportional (4x true scale) to the basal diameter of the cone (van Wyk de Vries et al., 2018). Yellow star marks the location of Deep Sea Drilling Project (DSDP) Site 270 (Ford and Barrett, 1975). (b) Thermal subsidence history since 34 Ma based on a simple 1D cooling model (McKenzie, 1978). Cumulative subsidence is measured as a percentage of the total post-34 Ma subsidence; the magnitude of subsidence is spatially variable (see panel a). A simplified geological timescale is provided for reference. Abbreviations: E=Eocene; PL=Pliocene; PE=Pleistocene; H=Holocene; Q=Quaternary.

Figure 9. S-wave velocity (Vs) model for central and West Antarctica (modified from Shen et al., 2018, with permission from John Wiley and Sons, ©2018). (a–d) Map views of Vs at four depth slices in the tomography model (depths are relative to a reference datum in the upper crust). Dashed lines mark the approximate limits of Marie Byrd Land and the West Antarctic Rift System. (e) Vertical slice of the 3D tomography model of the crust and upper mantle along transect X–Y (location marked on above panels). The Vs of the crust is plotted as absolute values, whereas the Vs of the mantle is shown as percentage perturbation relative to 4.4 km/sec; the Moho is marked by the solid line in the pofile. MBL = Marie Byrd Land; RIS = Ross Ice Shelf; TAM = Transantarctic Mountains; WARS = West Antarctic Rift System.

Figure 10. Mantle flow, dynamic topography, and ice sheet modelling in the Wilkes Subglacial Basin (modified from Austermann et al., 2015, with permission of the Geological Society of America, ©2015). (a and b) Present-day mantle temperature fields (perturbations relative to the global average) and computed mantle flow vectors for transects a–a' and b–b' crossing the Wilkes Subglacial Basin (profile locations indicated in panel c). (c) Change in dynamic topography since 3 Ma caused by the motion of the Antarctic plate through the mantle flow field. The plate rotation vector in the Wilkes Subglacial Basin is marked by white arrow, and has a magnitude of 1.6 cm/yr. (d and e) AIS surface elevation computed using simulations for mid-Pliocene climates which (d) do not include, and (e) do include, changes in dynamic topography since 3 Ma (panel c). (f) Difference in ice sheet thickness in the Wilkes Subglacial Basin (panel extent marked by dashed boxes in panels d and e) between the simulations shown in panels d and e.

Figure 11. Compensation of topography in Antarctica. (a) Present-day 'rock-equivalent' topography, whereby the ice sheet is converted into an equivalent mass of rock and added to the bed topography. Elevations are relative to mean sea level. (b) Isostatic topography, calculated from the seismic crustal thickness assuming local compensation (Airy isostasy) and a zero-elevation crustal thickness of 35 km for East Antarctica and 25 km for West Antarctica (An et al., 2015a). (c) Residual topography, calculated by subtracting the isostatic topography from the rock-equivalent topography. This represents topography that is not in Airy isostatic balance. While this imbalance may be due to dynamic support of topography by the mantle, it may arise due to flexural isostasy or variations in crustal density. The topography has been median filtered at 100 km to remove short-wavelength features unlikely to arise from mantle convection. (d) Long-wavelength (>3300 km) GOCE satellite

gravity anomaly (Bruinsma et al., 2014), which is scaled to dynamic topography using a uniform 'convective' admittance ratio of 30 mGal/km.

References

Aitken, A.R.A., Roberts, J.L., van Ommen, T.D., Young, D.A., Golledge, N.R., Greenbaum, J.S., Blankenship, D.D., Siegert, M.J., 2016. Repeated large-scale retreat and advance of Totten Glacier indicated by inland bed erosion. Nature 533, 385–389. doi:10.1038/nature17447

Al-Hajri, Y., White, N., Fishwick, S., 2009. Scales of transient convective support beneath Africa. Geology 37, 883–886. doi:10.1130/G25703A.1

An, M., Wiens, D.A., Zhao, Y., Feng, M., Nyblade, A.A., Kanao, M., Li, Y., Maggi, A., Lévêque, J.-J., 2015a. S-velocity model and inferred Moho topography beneath the Antarctic Plate from Rayleigh waves. J. Geophys. Res. Solid Earth 120, 359–383. doi:10.1002/2014JB011332

An, M., Wiens, D.A., Zhao, Y., Feng, M., Nyblade, A.A., Kanao, M., Li, Y., Maggi, A., Lévêque, J.-J., 2015b. Temperature, lithosphere-asthenosphere boundary, and heat flux beneath the Antarctic Plate inferred from seismic velocities. J. Geophys. Res. Solid Earth 120, 8720–8742. doi:10.1002/2015JB011917

Austermann, J., Pollard, D., Mitrovica, J.X., Moucha, R., Forte, A.M., DeConto, R.M., Rowley, D.B., Raymo, M.E., 2015. The impact of dynamic topography change on Antarctic ice sheet stability during the mid-Pliocene warm period. Geology 43, 927–930. doi:10.1130/G36988.1

Barletta, V.R., Bevis, M., Smith, B.E., Wilson, T., Brown, A., Bordoni, A., Willis, M., Khan, S.A., Rovira-Navarro, M., Dalziel, I., Smalley, R., Kendrick, E., Konfal, S., Caccamise, D.J., Aster, R.C., Nyblade, A., Wiens, D.A., 2018. Observed rapid bedrock uplift in Amundsen Sea Embayment promotes ice-sheet stability. Science 360, 1335–1339. doi:10.1126/science.aao1447

Barrett, P.J., 2008. A History of Antarctic Cenozoic Glaciation – View from the Margin, in: Florindo, F., Siegert, M.J. (Eds.), Developments in Earth and Environmental Sciences. Elsevier, pp. 33–83. doi:10.1016/S1571-9197(08)00003-7

Barrett, P.J., 1975. Textural characteristics of Cenozoic preglacial and glacial sediments at Site 270, Ross Sea, Antarctica. Initial Reports Deep Sea Drill. Proj. Leg 28 28, 757–767.

Behrendt, J.C., Blankenship, D.D., Finn, C.A., Bell, R.E., Sweeney, R.E., Hodge, S.M., Brozena, J.M., 1994. CASERTZ aeromagnetic data reveal late Cenozoic flood basalts(?) in the West Antarctic rift system. Geology 22, 527. doi:10.1130/0091-7613(1994)022<0527:CADRLC>2.3.CO;2

Behrendt, J.C., LeMasurier, W.E., Cooper, A.K., Tessensohn, F., Tréhu, A., Damaske, D., 1991. Geophysical studies of the West Antarctic Rift System. Tectonics 10, 1257–1273. doi:10.1029/91TC00868

Bell, R.E., Blankenship, D.D., Finn, C.A., Morse, D.L., Scambos, T.A., Brozena, J.M., Hodge, S.M., 1998. Influence of subglacial geology on the onset of a West Antarctic ice stream from aerogeophysical observations. Nature 394, 58–62. doi:10.1038/27883

Bentley, M.J., O'Cofaigh, C., Anderson, J.B., Conway, H., Davies, B., Graham, A.G.C., Hillenbrand, C.D., Hodgson, D.A., Jamieson, S.S.R., Larter, R.D., Mackintosh, A., Smith, J.A., Verleyen, E., Ackert, R.P., Bart, P.J., Berg, S., Brunstein, D., Canals, M., Colhoun, E.A., Crosta, X., Dickens, W.A., Domack, E., Dowdeswell, J.A., Dunbar, R., Ehrmann, W., Evans, J., Favier, V., Fink, D., Fogwill, C.J., Glasser, N.F., Gohl, K., Golledge, N.R., Goodwin, I., Gore, D.B., Greenwood, S.L., Hall, B.L., Hall, K., Hedding, D.W., Hein, A.S., Hocking, E.P., Jakobsson, M., Johnson, J.S., Jomelli, V., Jones, R.S., Klages, J.P., Kristoffersen, Y., Kuhn, G., Leventer, A., Licht, K., Lilly, K., Lindow, J., Livingstone, S.J., Massé, G., McGlone, M.S., McKay, R.M., Melles, M., Miura, H., Mulvaney, R., Nel, W., Nitsche, F.O., O'Brien, P.E., Post, A.L., Roberts, S.J., Saunders, K.M., Selkirk, P.M., Simms, A.R., Spiegel, C., Stolldorf, T.D., Sugden, D.E., van der Putten, N., van Ommen, T., Verfaillie, D., Vyverman, W., Wagner, B., White, D.A., Witus, A.E., Zwartz, D., 2014. A community-based geological reconstruction of Antarctic Ice Sheet deglaciation since the Last Glacial Maximum. Quat. Sci. Rev. 100, 1–9. doi:10.1016/j.quascirev.2014.06.025

Bialas, R.W., Buck, W.R., Studinger, M., Fitzgerald, P.G., 2007. Plateau collapse model for the Transantarctic Mountains-West Antarctic Rift System: Insights from numerical experiments. Geology 35, 687–690. doi:10.1130/G23825A.1

Bingham, R.G., Ferraccioli, F., King, E.C., Larter, R.D., Pritchard, H.D., Smith, A.M., Vaughan, D.G., 2012. Inland thinning of West Antarctic Ice Sheet steered along subglacial rifts. Nature 487, 468–471. doi:10.1038/nature11292

Block, A.E., Bell, R.E., Studinger, M., 2009. Antarctic crustal thickness from satellite gravity: Implications for the Transantarctic and Gamburtsev Subglacial Mountains. Earth Planet. Sci. Lett. 288, 194–203. doi:10.1016/j.epsl.2009.09.022

Boger, S.D., 2011. Antarctica — Before and after Gondwana. Gondwana Res. 19, 335–371. doi:10.1016/j.gr.2010.09.003

Braun, J., 2010. The many surface expressions of mantle dynamics. Nat. Geosci. 3, 825–833. doi:10.1038/ngeo1020

Brenn, G.R., Hansen, S.E., Park, Y., 2017. Variable thermal loading and flexural uplift along the Transantarctic Mountains, Antarctica. Geology 45, 463–466. doi:10.1130/G38784.1

Bruinsma, S.L., Förste, C., Abrikosov, O., Lemoine, J.-M., Marty, J.-C., Mulet, S., Rio, M.-H., Bonvalot, S., 2014. ESA's satellite-only gravity field model via the direct approach based on all GOCE data. Geophys. Res. Lett. 41, 7508–7514. doi:10.1002/2014GL062045

Burton-Johnson, A., Black, M., Peter, T.F., Kaluza-Gilbert, J., 2016. An automated methodology for differentiating rock from snow, clouds and sea in Antarctica from Landsat 8 imagery: A new rock outcrop map and area estimation for the entire Antarctic continent. Cryosph. 10, 1665–1677. doi:10.5194/tc-10-1665-2016

Cande, S.C., Stock, J.M., Müller, R.D., Ishihara, T., 2000. Cenozoic motion between East and West Antarctica. Nature 404, 145–150. doi:10.1038/35004501

Carter, A., Riley, T.R., Hillenbrand, C.-D., Rittner, M., 2017. Widespread Antarctic glaciation during the Late Eocene. Earth Planet. Sci. Lett. 458, 49–57. doi:10.1016/j.epsl.2016.10.045

Cazenave, A., Souriau, A., Dominh, K., 1989. Global coupling of Earth surface topography with hotspots, geoid and mantle heterogeneities. Nature 340, 54–57. doi:10.1038/340054a0

Chaput, J., Aster, R.C., Huerta, A., Sun, X., Lloyd, A., Wiens, D., Nyblade, A., Anandakrishnan, S., Winberry, J.P., Wilson, T., 2014. The crustal thickness of West Antarctica. J. Geophys. Res. Solid Earth 119, 378–395. doi:10.1002/2013JB010642

Chen, B., Haeger, C., Kaban, M.K., Petrunin, A.G., 2018. Variations of the effective elastic thickness reveal tectonic fragmentation of the Antarctic lithosphere. Tectonophysics 746, 412–424. doi:10.1016/j.tecto.2017.06.012

Clerc, F., Minchew, B.M., Behn, M.D., 2019. Marine Ice Cliff Instability Mitigated by Slow Removal of Ice Shelves. Geophys. Res. Lett. 46, 12108–12116. doi:10.1029/2019GL084183

Coenen, J.J., Scherer, R., Baudoin, P., Warny, S., Castañeda, I.S., Askin, R., 2019. Paleogene marine and terrestrial development of the West Antarctic Rift System. Geophys. Res. Lett. doi:10.1029/2019GL085281

Colleoni, F., De Santis, L., Montoli, E., Olivo, E., Sorlien, C.C., Bart, P.J., Gasson, E.G.W., Bergamasco, A., Sauli, C., Wardell, N., Prato, S., 2018. Past continental shelf evolution increased Antarctic ice sheet sensitivity to climatic conditions. Sci. Rep. 8, 11323. doi:10.1038/s41598-018-29718-7

Colli, L., Ghelichkhan, S., Bunge, H.P., 2016. On the ratio of dynamic topography and gravity anomalies in a dynamic Earth. Geophys. Res. Lett. 43, 2510–2516. doi:10.1002/2016GL067929

Cox, S.E., Thomson, S.N., Reiners, P.W., Hemming, S.R., van de Flierdt, T., 2010. Extremely

low long-term erosion rates around the Gamburtsev Mountains in interior East Antarctica. Geophys. Res. Lett. 37. doi:10.1029/2010GL045106

Coxall, H.K., Wilson, P.A., Pälike, H., Lear, C.H., Backman, J., 2005. Rapid stepwise onset of Antarctic glaciation and deeper calcite compensation in the Pacific Ocean. Nature 433, 53–57. doi:10.1038/nature03135

Czarnota, K., Hoggard, M.J., White, N., Winterbourne, J., 2013. Spatial and temporal patterns of Cenozoic dynamic topography around Australia. Geochemistry, Geophys. Geosystems 14, 634–658. doi:10.1029/2012GC004392

Dalziel, I.W.D., 1997. Neoproterozoic-Paleozoic geography and tectonics : Review, hypothesis, environmental speculation. Geol. Soc. Am. Bull. 109, 16–42.

De Santis, L., Prato, S., Brancolini, G., Lovo, M., Torelli, L., 1999. The Eastern Ross Sea continental shelf during the Cenozoic: Implications for the West Antarctic ice sheet development. Glob. Planet. Change 23, 173–196. doi:10.1016/S0921-8181(99)00056-9

Decesari, R.C., Wilson, D.S., Luyendyk, B.P., Faulkner, M., 2007. Cretaceous and Tertiary extension throughout the Ross Sea, Antarctica, in: Cooper, A.K. (Ed.), Antarctica: A Keystone in a Changing World – Online Proceedings of the 10th ISAES. U.S. Geol. Surv. Open File Rep., 2007–1047. doi:10.3133/of2007-1047.srp098

DeConto, R.M., Pollard, D., 2016. Contribution of Antarctica to past and future sea-level rise. Nature 531, 591–597. doi:10.1038/nature17145

DeConto, R.M., Pollard, D., 2003a. Rapid Cenozoic glaciation of Antarctica induced by declining atmospheric CO2. Nature 421, 245–249. doi:10.1038/nature01290

DeConto, R.M., Pollard, D., 2003b. A coupled climate–ice sheet modeling approach to the Early Cenozoic history of the Antarctic ice sheet. Palaeogeogr. Palaeoclimatol. Palaeoecol. 198, 39–52. doi:10.1016/S0031-0182(03)00393-6

DeConto, R.M., Pollard, D., Wilson, P.A., Pälike, H., Lear, C.H., Pagani, M., 2008. Thresholds for Cenozoic bipolar glaciation. Nature 455, 652–656. doi:10.1038/nature07337

Drewry, D.J., 1983. Antarctica: Glaciological and Geophysical Folio. Scott Polar Research Institute, University of Cambridge.

Ebbing, J., Haas, P., Ferraccioli, F., Pappa, F., Szwillus, W., Bouman, J., 2018. Earth tectonics as seen by GOCE - Enhanced satellite gravity gradient imaging. Sci. Rep. 8, 16356. doi:10.1038/s41598-018-34733-9

Edwards, T.L., Brandon, M.A., Durand, G., Edwards, N.R., Golledge, N.R., Holden, P.B., Nias, I.J., Payne, A.J., Ritz, C., Wernecke, A., 2019. Revisiting Antarctic ice loss due to marine ice-cliff instability. Nature 566, 58–64. doi:10.1038/s41586-019-0901-4

Elliot, D.H., Fleming, T.H., 2004. Occurrence and dispersal of magmas in the Jurassic Ferrar Large Igneous Province, Antarctica. Gondwana Res. 7, 223–237. doi:10.1016/S1342-937X(05)70322-1

Ferraccioli, F., Armadillo, E., Zunino, A., Bozzo, E., Rocchi, S., Armienti, P., 2009. Magmatic and tectonic patterns over the Northern Victoria Land sector of the Transantarctic Mountains from new aeromagnetic imaging. Tectonophysics 478, 43–61. doi:10.1016/j.tecto.2008.11.028

Ferraccioli, F., Finn, C.A., Jordan, T.A., Bell, R.E., Anderson, L.M., Damaske, D., 2011. East Antarctic rifting triggers uplift of the Gamburtsev Mountains. Nature 479, 388–392. doi:10.1038/nature10566

Finn, C.A., Müller, R.D., Panter, K.S., 2005. A Cenozoic diffuse alkaline magmatic province (DAMP) in the southwest Pacific without rift or plume origin. Geochemistry, Geophys. Geosystems 6. doi:10.1029/2004GC000723

Flament, N., Gurnis, M., Muller, R.D., 2013. A review of observations and models of dynamic topography. Lithosphere 5, 189–210. doi:10.1130/L245.1

Ford, A.B., Barrett, P.J., 1975. Basement rocks of the south-central Ross Sea, Site 270, DSDP Leg 28. Initial Reports Deep Sea Drill. Proj. Leg 28 28, 861–868.

Forsberg, R., Olesen, A. V, Ferraccioli, F., Jordan, T.A., Matsuoka, K., Zakrajsek, A., Ghidella, M., Greenbaum, J.S., 2018. Exploring the Recovery Lakes region and interior Dronning Maud Land, East Antarctica, with airborne gravity, magnetic and radar measurements. Geol. Soc. London, Spec. Publ. 461. doi:10.1144/SP461.17

Forte, A.M., Peltier, W.R., Dziewonski, A.M., Woodward, R.L., 1993. Dynamic surface topography: A new interpretation based upon mantle flow models derived from seismic tomography. Geophys. Res. Lett. 20, 225–228. doi:10.1029/93GL00249

Fretwell, P., Pritchard, H.D., Vaughan, D.G., Bamber, J.L., Barrand, N.E., Bell, R., Bianchi, C., Bingham, R.G., Blankenship, D.D., Casassa, G., Catania, G., Callens, D., Conway, H., Cook, A.J., Corr, H.F.J., Damaske, D., Damm, V., Ferraccioli, F., Forsberg, R., Fujita, S., Gim, Y., Gogineni, P., Griggs, J.A., Hindmarsh, R.C.A., Holmlund, P., Holt, J.W., Jacobel, R.W., Jenkins, A., Jokat, W., Jordan, T., King, E.C., Kohler, J., Krabill, W., Riger-Kusk, M., Langley, K.A., Leitchenkov, G., Leuschen, C., Luyendyk, B.P., Matsuoka, K., Mouginot, J., Nitsche, F.O., Nogi, Y., Nost, O.A., Popov, S. V., Rignot, E., Rippin, D.M., Rivera, A., Roberts, J., Ross, N., Siegert, M.J., Smith, A.M., Steinhage, D., Studinger, M., Sun, B., Tinto, B.K., Welch, B.C., Wilson, D., Young, D.A., Xiangbin, C., Zirizzotti, A., 2013. Bedmap2: improved ice bed, surface and thickness datasets for Antarctica. Cryosph. 7, 375–393. doi:10.5194/tc-7-375-2013

Gasson, E., DeConto, R.M., Pollard, D., 2015. Antarctic bedrock topography uncertainty and

ice sheet stability. Geophys. Res. Lett. 42, 5372–5377. doi:10.1002/2015GL064322

Gasson, E., DeConto, R.M., Pollard, D., Levy, R.H., 2016. Dynamic Antarctic ice sheet during the early to mid-Miocene. Proc. Natl. Acad. Sci. 113, 3459–3464. doi:10.1073/pnas.1516130113

Gohl, K., 2008. Antarctica's Continent-Ocean Transitions : Consequences for Tectonic Reconstructions, in: Cooper, A.K., Barrett, P.J., Stagg, H.M.J., Storey, B.C., Stump, E., Wise, W. (Eds.), Antarctica: A Keystone in a Changing World - Online Proceedings of the 10th ISAES. The National Academies Press, Washington, D.C., pp. 29–38. doi:10.3133/of2007-1047.kp04

Golledge, N.R., Kowalewski, D.E., Naish, T.R., Levy, R.H., Fogwill, C.J., Gasson, E.G.W., 2015. The multi-millennial Antarctic commitment to future sea-level rise. Nature 526, 421–425. doi:10.1038/nature15706

Gomez, N., Mitrovica, J.X., Huybers, P., Clark, P.U., 2010. Sea level as a stabilizing factor for marine-ice-sheet grounding lines. Nat. Geosci. 3, 850–853. doi:10.1038/ngeo1012

Granot, R., Dyment, J., 2018. Late Cenozoic unification of East and West Antarctica. Nat. Commun. 9, 3189. doi:10.1038/s41467-018-05270-w

Hager, B.H., Clayton, R.W., Richards, M.A., Comer, R.P., Dziewonski, A.M., 1985. Lower mantle heterogeneity, dynamic topography and the geoid. Nature 314, 752–752. doi:10.1038/314752a0

Hambrey, M.J., Ehrmann, W.U., Larsen, B., 1991. Cenozoic Glacial Record of the Prydz Bay Continental Shelf, East Antarctica, in: Proceedings of the Ocean Drilling Program, 119 Scientific Results. Ocean Drilling Program, pp. 77–132. doi:10.2973/odp.proc.sr.119.200.1991

Hansen, S.E., Kenyon, L.M., Graw, J.H., Park, Y., Nyblade, A.A., 2016. Crustal structure beneath the Northern Transantarctic Mountains and Wilkes Subglacial Basin: Implications for tectonic origins. J. Geophys. Res. Solid Earth 121, 812–825. doi:10.1002/2015JB012325

Hansen, S.E., Nyblade, A.A., Heeszel, D.S., Wiens, D.A., Shore, P., Kanao, M., 2010. Crustal structure of the Gamburtsev Mountains, East Antarctica, from S-wave receiver functions and Rayleigh wave phase velocities. Earth Planet. Sci. Lett. 300, 395–401. doi:10.1016/j.epsl.2010.10.022

Hoggard, M.J., White, N., Al-Attar, D., 2016. Global dynamic topography observations reveal limited influence of large-scale mantle flow. Nat. Geosci. 9, 456–463. doi:10.1038/ngeo2709

Hoggard, M.J., Winterbourne, J., Czarnota, K., White, N., 2017. Oceanic residual depth

measurements, the plate cooling model, and global dynamic topography. J. Geophys. Res. Solid Earth 122, 2328–2372. doi:10.1002/2016JB013457

Hole, M.J., LeMasurier, W.E., 1994. Tectonic controls on the geochemical composition of Cenozoic, mafic alkaline volcanic rocks from West Antarctica. Contrib. to Mineral. Petrol. 117, 187–202. doi:10.1007/BF00286842

Huerta, A.D., 2007. Byrd drainage system; evidence of a Mesozoic West Antarctic plateau, in: Cooper, A.K., Raymond, C.R. (Eds.), Antarctica: A Keystone in a Changing World – Online Proceedings of the 10th ISAES X: USGS Open-File Report 2007-1047. p. Extended Abstract 091, 5 p.

Humbert, A., Steinhage, D., Helm, V., Beyer, S., Kleiner, T., 2018. Missing Evidence of Widespread Subglacial Lakes at Recovery Glacier, Antarctica. J. Geophys. Res. Earth Surf. doi:10.1029/2017JF004591

Jamieson, S.S.R., Hulton, N.R.J., Hagdorn, M., 2008. Modelling landscape evolution under ice sheets. Geomorphology 97, 91–108. doi:10.1016/j.geomorph.2007.02.047

Jamieson, S.S.R., Hulton, N.R.J., Sugden, D.E., Payne, A.J., Taylor, J., 2005. Cenozoic landscape evolution of the Lambert basin, East Antarctica: the relative role of rivers and ice sheets. Glob. Planet. Change 45, 35–49. doi:10.1016/j.gloplacha.2004.09.015

Jamieson, S.S.R., Stokes, C.R., Ross, N., Rippin, D.M., Bingham, R.G., Wilson, D.S., Margold, M., Bentley, M.J., 2014. The glacial geomorphology of the Antarctic ice sheet bed. Antarct. Sci. 26, 724–741. doi:10.1017/S0954102014000212

Jamieson, S.S.R., Sugden, D.E., 2008. Landscape Evolution of Antarctica, in: Cooper, A.K., Barrett, P.J., Stagg, H., Storey, B., Stump, E., Wise, W. (Eds.), Antarctica: A Keystone in a Changing World. The National Academies Press, Washington DC, pp. 39–54. doi:10.1007/s13398-014-0173-7.2

Jamieson, S.S.R., Sugden, D.E., Hulton, N.R.J., 2010. The evolution of the subglacial landscape of Antarctica. Earth Planet. Sci. Lett. 293, 1–27. doi:10.1016/j.epsl.2010.02.012

Japsen, P., Bonow, J.M., Green, P.F., Chalmers, J.A., Lidmar-Bergström, K., 2006. Elevated, passive continental margins: Long-term highs or Neogene uplifts? New evidence from West Greenland. Earth Planet. Sci. Lett. 248, 330–339. doi:10.1016/j.epsl.2006.05.036

Ji, F., Gao, J., Shen, Z., Zhang, Q., Li, Y., 2017. Variations of the effective elastic thickness over the Ross Sea and Transantarctic Mountains and implications for their structure and tectonics. Tectonophysics 717, 127–138. doi:10.1016/j.tecto.2017.07.011

Jordan, T.A., Ferraccioli, F., Armadillo, E., Bozzo, E., 2013. Crustal architecture of the Wilkes Subglacial Basin in East Antarctica, As revealed from airborne gravity data.

Tectonophysics 585, 196–206. doi:10.1016/j.tecto.2012.06.041

Jordan, T.A., Ferraccioli, F., Leat, P.T., 2017. New geophysical compilations link crustal block motion to Jurassic extension and strike-slip faulting in the Weddell Sea Rift System of West Antarctica. Gondwana Res. 42, 29–48. doi:10.1016/j.gr.2016.09.009

Jordan, T.A., Ferraccioli, F., Vaughan, D.G., Holt, J.W., Corr, H., Blankenship, D.D., Diehl, T.M., 2010. Aerogravity evidence for major crustal thinning under the Pine Island Glacier region (West Antarctica). Bull. Geol. Soc. Am. 122, 714–726. doi:10.1130/B26417.1

Jordan, T.A., Martin, C., Ferraccioli, F., Matsuoka, K., Corr, H., Forsberg, R., Olesen, A., Siegert, M.J., 2018. Anomalously high geothermal flux near the South Pole. Sci. Rep. 8, 16785. doi:10.1038/s41598-018-35182-0

Joughin, I., Alley, R.B., 2011. Stability of the West Antarctic ice sheet in a warming world. Nat. Geosci. 4, 506–513. doi:10.1038/ngeo1194

Karlsson, N.B., Binder, T., Eagles, G., Helm, V., Pattyn, F., Van Liefferinge, B., Eisen, O., 2018. Glaciological characteristics in the Dome Fuji region and new assessment for "Oldest Ice." Cryosph. 12, 2413–2424. doi:10.5194/tc-12-2413-2018

Karner, G.D., Studinger, M., Bell, R.E., 2005. Gravity anomalies of sedimentary basins and their mechanical implications: Application to the Ross Sea basins, West Antarctica. Earth Planet. Sci. Lett. 235, 577–596. doi:10.1016/j.epsl.2005.04.016

Katz, M.E., Miller, K.G., Wright, J.D., Wade, B.S., Browning, J. V., Cramer, B.S., Rosenthal, Y., 2008. Stepwise transition from the Eocene greenhouse to the Oligocene icehouse. Nat. Geosci. 1, 329–334. doi:10.1038/ngeo179

Kennett, J.P., 1977. Cenozoic evolution of Antarctic glaciation, the circum-Antarctic Ocean, and their impact on global paleoceanography. J. Geophys. Res. 82, 3843–3860. doi:10.1029/JC082i027p03843

Kessler, M.A., Anderson, R.S., Briner, J.P., 2008. Fjord insertion into continental margins driven by topographic steering of ice. Nat. Geosci. 1, 365–369. doi:10.1038/ngeo201

Kingslake, J., Scherer, R.P., Albrecht, T., Coenen, J., Powell, R.D., Reese, R., Stansell, N.D., Tulaczyk, S., Wearing, M.G., Whitehouse, P.L., 2018. Extensive retreat and re-advance of the West Antarctic Ice Sheet during the Holocene. Nature 558, 430–434. doi:10.1038/s41586-018-0208-x

Kirby, J.F., 2014. Estimation of the effective elastic thickness of the lithosphere using inverse spectral methods: The state of the art. Tectonophysics 631, 87–116. doi:10.1016/j.tecto.2014.04.021

Koppes, M.N., Montgomery, D.R., 2009. The relative efficacy of fluvial and glacial erosion over modern to orogenic timescales. Nat. Geosci. 2, 644–647. doi:10.1038/ngeo616

Krohne, N., Lisker, F., Kleinschmidt, G., Klugel, A., Laufer, A., Estrada, S., Spiegel, C., 2016. The Shackleton Range (East Antarctica): an alien block at the rim of Gondwana? Geol. Mag. 1–24. doi:10.1017/S0016756816001011

Kulhanek, D.K., Levy, R.H., Clowes, C.D., Prebble, J.G., Rodelli, D., Jovane, L., Morgans, H.E.G., Kraus, C., Zwingmann, H., Griffith, E.M., Scher, H.D., McKay, R.M., Naish, T.R., 2019. Revised chronostratigraphy of DSDP Site 270 and late Oligocene to early Miocene paleoecology of the Ross Sea sector of Antarctica. Glob. Planet. Change 178, 46–64. doi:10.1016/j.gloplacha.2019.04.002

Lawrence, J.F., Wiens, D.A., Nyblade, A.A., Anandakrishnan, S., Shore, P.J., Voigt, D., 2006. Crust and upper mantle structure of the Transantarctic Mountains and surrounding regions from receiver functions, surface waves, and gravity: Implications for uplift models. Geochemistry, Geophys. Geosystems 7. doi:10.1029/2006GC001282

Leckie, R.M., Webb, P.-N., 1983. Late Oligocene-early Miocene glacial record of the Ross Sea, Antarctica : Evidence from DSDP Site 270. Geology 11, 578–582.

LeMasurier, W.E., Landis, C.A., 1996. Mantle-plume activity recorded by low-relief erosion surfaces in West Antarctica and New Zealand. Bull. Geol. Soc. Am. 108, 1450–1466. doi:10.1130/0016-7606(1996)108<1450:MPARBL>2.3.CO;2

LeMasurier, W.E., Rex, D.C., 1989. Evolution of linear volcanic ranges in Marie Byrd Land, West Antarctica. J. Geophys. Res. 94, 7223. doi:10.1029/JB094iB06p07223

LeMasurier, W.E., Thomson, J.W., Baker, P.E., Kyle, P.R., Rowley, P.D., Smellie, J.L., Verwoerd, W.J. (Eds.), 1990. Volcanoes of the Antarctic Plate and Southern Oceans, Antarctic Research Series. American Geophysical Union, Washington, D. C. doi:10.1029/AR048

Leuschen, C., Gogineni, P., Rodriguez-Morales, F., Paden, J., Allen, C., 2016. IceBridge MCoRDS L2 Ice Thickness, Version 1. Boulder, Color. USA. NASA Natl. Snow Ice Data Cent. Distrib. Act. Arch. Cent.

Liu, Z., Pagani, M., Zinniker, D., Deconto, R.M., Huber, M., Brinkhuis, H., Shah, S.R., Leckie, R.M., Pearson, A., 2009. Global cooling during the Eocene-Oligocene climate transition. Science 323, 1187–1190. doi:10.1126/science.1166368

Lloyd, A.J., Wiens, D.A., Nyblade, A.A., Anandakrishnan, S., Aster, R.C., Huerta, A.D., Wilson, T.J., Dalziel, I.W.D., Shore, P.J., Zhao, D., 2015. A seismic transect across West Antarctica: Evidence for mantle thermal anomalies beneath the Bentley Subglacial Trench and the Marie Byrd Land Dome. J. Geophys. Res. Solid Earth 120, 8439–8460.

doi:10.1002/2015JB012455

Lloyd, A.J., Wiens, D.A., Zhu, H., Tromp, J., Nyblade, A.A., Aster, R.C., Hansen, S.E., Dalziel, I.W.D., Wilson, T.J., Ivins, E.R., O'Donnell, J.P., 2020. Seismic Structure of the Antarctic Upper Mantle Imaged with Adjoint Tomography. J. Geophys. Res. Solid Earth 125, 2019JB017823. doi:10.1029/2019JB017823

Lythe, M., Vaughan, D.G., Lambrecht, A., Miller, H., Nixdorf, U., Oerter, H., Steinhage, D., Allison, I.F., Craven, M., Goodwin, I.D., Jacka, J., Morgan, V., Ruddell, A., Young, N., Wellman, P., Cooper, A.P.R., Corr, H.F.J., Doake, C.S.M., Hindmarsh, R.C.A., Jenkins, A., Johnson, M.R., Jones, P., King, E.C., Smith, A.M., Thomson, J.W., Thorley, M.R., Jezek, K., Li, B., Liu, H., Damm, V., Nishio, F., Fujita, S., Skvarca, P., Remy, F., Testut, L., Sievers, J., Kapitsa, A., Macheret, Y., Scambos, T., Filina, I., Masolov, V., Popov, S., Johnstone, G., Jacobel, B., Holmlund, P., Naslund, J., Anandakrishnan, S., Bamber, J.L., Bassford, R., Decleir, H., Huybrechts, P., Rivera, A., Grace, N., Casassa, G., Tabacco, I., Blankenship, D., Morse, D., Gades, T., Nereson, N., Bentley, C.R., Lord, N., Lange, M., Sandhäger, H., 2001. BEDMAP: a new ice thickness and subglacial topographic model of Antarctica. J. Geophys. Res. 106, 11335–11351. doi:10.1029/2000JB900449

Maritati, A., Aitken, A.R.A., Young, D.A., Roberts, J.L., Blankenship, D.D., Siegert, M.J., 2016. The tectonic development and erosion of the Knox Subglacial Sedimentary Basin, East Antarctica. Geophys. Res. Lett. 1–10. doi:10.1002/2016GL071063

McKenzie, D., 2010. The influence of dynamically supported topography on estimates of Te. Earth Planet. Sci. Lett. 295, 127–138. doi:10.1016/j.epsl.2010.03.033

McKenzie, D., 1994. The Relationship between Topography and Gravity on Earth and Venus. Icarus. doi:10.1006/icar.1994.1170

McKenzie, D., 1978. Some Remarks on Development of Sedimentary Basins. Earth Planet. Sci. Lett. 40, 25–32. doi:10.1016/0012-821x(78)90071-7

McKenzie, D., Fairhead, D., 1997. Estimates of the effective elastic thickness of the continental lithosphere from Bouguer and free air gravity anomalies. J. Geophys. Res. 102, 27523–27552. doi:10.1029/97JB02481

McKenzie, D.P., Roberts, J.M., Weiss, N.O., 1974. Convection in the earth's mantle: Towards a numerical simulation. J. Fluid Mech. 62, 465–538. doi:10.1017/S0022112074000784

Menard, H.W., 1973. Depth anomalies and the bobbing motion of drifting islands. J. Geophys. Res. 78, 5128–5137. doi:10.1029/jb078i023p05128

Mengel, M., Levermann, A., 2014. Ice plug prevents irreversible discharge from East Antarctica. Nat. Clim. Chang. 4, 451–455. doi:10.1038/nclimate2226

Mercer, J.H., 1978. West Antarctic ice sheet and CO2 greenhouse effect: a threat of disaster.

Nature 271, 321–325. doi:10.1073/pnas.0703993104

Molnar, P., England, P., 1990. Late Cenozoic uplift of mountain ranges and global climate change: chicken or egg? Nature 346, 29–34. doi:10.1038/346029a0

Molnar, P., England, P.C., Jones, C.H., 2015. Mantle dynamics, isostasy, and the support of high terrain. J. Geophys. Res. Solid Earth 120, 1–26. doi:10.1002/2014JB011724

Morlighem, M., Rignot, E., Binder, T., Blankenship, D., Drews, R., Eagles, G., Eisen, O., Ferraccioli, F., Forsberg, R., Fretwell, P., Goel, V., Greenbaum, J.S., Gudmundsson, H., Guo, J., Helm, V., Hofstede, C., Howat, I., Humbert, A., Jokat, W., Karlsson, N.B., Lee, W.S., Matsuoka, K., Millan, R., Mouginot, J., Paden, J., Pattyn, F., Roberts, J., Rosier, S., Ruppel, A., Seroussi, H., Smith, E.C., Steinhage, D., Sun, B., Broeke, M.R. van den, Ommen, T.D. van, Wessem, M. van, Young, D.A., 2019. Deep glacial troughs and stabilizing ridges unveiled beneath the margins of the Antarctic ice sheet. Nat. Geosci. doi:10.1038/s41561-019-0510-8

Müller, R.D., Seton, M., Zahirovic, S., Williams, S.E., Matthews, K.J., Wright, N.M., Shephard, G.E., Maloney, K.T., Barnett-Moore, N., Hosseinpour, M., Bower, D.J., Cannon, J., 2016. Ocean Basin Evolution and Global-Scale Plate Reorganization Events Since Pangea Breakup. Annu. Rev. Earth Planet. Sci. 44, 107–138. doi:10.1146/annurev-earth-060115-012211

Naish, T.R., Woolfe, K.J., Barrett, P.J., Wilson, G.S., Atkins, C., Bohaty, S.M., Bücker, C.J., Claps, M., Davey, F.J., Dunbar, G.B., Dunn, A.G., Fielding, C.R., Florindo, F., Hannah, M.J., Harwood, D.M., Henrys, S.A., Krissek, L.A., Lavelle, M., van Der Meer, J., McIntosh, W.C., Niessen, F., Passchier, S., Powell, R.D., Roberts, A.P., Sagnotti, L., Scherer, R.P., Strong, C.P., Talarico, F., Verosub, K.L., Villa, G., Watkins, D.K., Webb, P.N., Wonik, T., 2001. Orbitally induced oscillations in the East Antarctic ice sheet at the Oligocene/Miocene boundary. Nature 413, 719–23. doi:10.1038/35099534

O'Donnell, J.P., Nyblade, A.A., 2014. Antarctica's hypsometry and crustal thickness: Implications for the origin of anomalous topography in East Antarctica. Earth Planet. Sci. Lett. 388, 143–155. doi:10.1016/j.epsl.2013.11.051

Olivetti, V., Rossetti, F., Balestrieri, M.L., Pace, D., Cornamusini, G., Talarico, F., 2018. Variability in uplift, exhumation and crustal deformation along the Transantarctic Mountains front in southern Victoria Land, Antarctica. Tectonophysics 745, 229–244. doi:10.1016/j.tecto.2018.08.017

Pagani, M., Huber, M., Liu, Z., Bohaty, S.M., Henderiks, J., Sijp, W., Krishnan, S., DeConto, R.M., 2011. The Role of Carbon Dioxide During the Onset of Antarctic Glaciation. Science 334, 1261–1264. doi:10.1126/science.1203909

Pappa, F., Ebbing, J., Ferraccioli, F., 2019. Moho Depths of Antarctica: Comparison of

Seismic, Gravity, and Isostatic Results. Geochemistry, Geophys. Geosystems 20, 1629–1645. doi:10.1029/2018GC008111

Passchier, S., Ciarletta, D.J., Miriagos, T.E., Bijl, P.K., Bohaty, S.M., 2017. An Antarctic stratigraphic record of stepwise ice growth through the Eocene-Oligocene transition. Geol. Soc. Am. Bull. 129, 318–330. doi:10.1130/B31482.1

Paxman, G.J.G., Jamieson, S.S.R., Ferraccioli, F., Bentley, M.J., Forsberg, R., Ross, N., Watts, A.B., Corr, H.F.J., Jordan, T.A., 2017. Uplift and tilting of the Shackleton Range in East Antarctica driven by glacial erosion and normal faulting. J. Geophys. Res. Solid Earth 122, 2390–2408. doi:10.1002/2016JB013841

Paxman, G.J.G., Jamieson, S.S.R., Ferraccioli, F., Bentley, M.J., Ross, N., Armadillo, E., Gasson, E.G.W., Leitchenkov, G., DeConto, R.M., 2018. Bedrock erosion surfaces record former East Antarctic Ice Sheet extent. Geophys. Res. Lett. 45, 4114–4123. doi:10.1029/2018GL077268

Paxman, G.J.G., Jamieson, S.S.R., Ferraccioli, F., Bentley, M.J., Ross, N., Watts, A.B., Leitchenkov, G., Armadillo, E., Young, D.A., 2019a. The role of lithospheric flexure in the landscape evolution of the Wilkes Subglacial Basin and Transantarctic Mountains, East Antarctica. J. Geophys. Res. Earth Surf. 124, 812–829. doi:10.1029/2018JF004705

Paxman, G.J.G., Jamieson, S.S.R., Hochmuth, K., Gohl, K., Bentley, M.J., Leitchenkov, G., Ferraccioli, F., 2019b. Reconstructions of Antarctic topography since the Eocene–Oligocene boundary. Palaeogeogr. Palaeoclimatol. Palaeoecol. 535, 109346. doi:10.1016/j.palaeo.2019.109346

Paxman, G.J.G., Watts, A.B., Ferraccioli, F., Jordan, T.A., Bell, R.E., Jamieson, S.S.R., Finn, C.A., 2016. Erosion-driven uplift in the Gamburtsev Subglacial Mountains of East Antarctica. Earth Planet. Sci. Lett. 452, 1–14. doi:10.1016/j.epsl.2016.07.040

Pearson, P.N., Foster, G.L., Wade, B.S., 2009. Atmospheric carbon dioxide through the Eocene–Oligocene climate transition. Nature 461, 1110–1113. doi:10.1038/nature08447

Pekeris, C.L., 1935. Thermal Convection in the Interior of the Earth. Geophys. J. Int. 3, 343–367. doi:10.1111/j.1365-246X.1935.tb01742.x

Pollard, D., DeConto, R.M., 2019. Continuous simulations over the last 40 million years with a coupled Antarctic ice sheet-sediment model. Palaeogeogr. Palaeoclimatol. Palaeoecol. 537, 109374. doi:10.1016/J.PALAEO.2019.109374

Pollard, D., DeConto, R.M., 2009. Modelling West Antarctic ice sheet growth and collapse through the past five million years. Nature 458, 329–332. doi:10.1038/nature07809

Pollard, D., DeConto, R.M., Alley, R.B., 2015. Potential Antarctic Ice Sheet retreat driven by

hydrofracturing and ice cliff failure. Earth Planet. Sci. Lett. 412, 112–121. doi:10.1016/j.epsl.2014.12.035

Quigley, M.C., Clark, D., Sandiford, M., 2010. Tectonic geomorphology of Australia. Geol. Soc. London, Spec. Publ. 346, 243–265. doi:10.1144/SP346.13

Ramirez, C., Nyblade, A., Hansen, S.E., Wiens, D.A., Anandakrishnan, S., Aster, R.C., Huerta, A.D., Shore, P., Wilson, T., 2016. Crustal and upper-mantle structure beneath ice-covered regions in Antarctica from S-wave receiver functions and implications for heat flow. Geophys. J. Int. 204, 1636–1648. doi:10.1093/gji/ggv542

Reusch, D.N., 2011. New Caledonian carbon sinks at the onset of Antarctic glaciation. Geology 39, 807–810. doi:10.1130/G31981.1

Richards, F.D., Hoggard, M.J., White, N.J., 2016. Cenozoic epeirogeny of the Indian peninsula. Geochemistry, Geophys. Geosystems 17, 4920–4954. doi:10.1002/2016GC006545

Rignot, E., Bamber, J.L., van den Broeke, M.R., Davis, C., Li, Y., van de Berg, W.J., van Meijgaard, E., 2008. Recent Antarctic ice mass loss from radar interferometry and regional climate modelling. Nat. Geosci. 1, 106–110. doi:10.1038/ngeo102

Rocchi, S., Armienti, P., D'Orazio, M., Tonarini, S., Wijbrans, J.R., Di Vincenzo, G., 2002. Cenozoic magmatism in the western Ross Embayment: Role of mantle plume versus plate dynamics in the development of the West Antarctic Rift System. J. Geophys. Res. Solid Earth 107. doi:10.1029/2001JB000515

Rocchi, S., LeMasurier, W.E., Di Vincenzo, G., 2006. Oligocene to Holocene erosion and glacial history in Marie Byrd Land, West Antarctica, inferred from exhumation of the Dorrel Rock intrusive complex and from volcano morphologies. Geol. Soc. Am. Bull. 118, 991–1005. doi:10.1130/B25675.1

Rose, K.C., Ferraccioli, F., Jamieson, S.S.R., Bell, R.E., Corr, H.F.J., Creyts, T.T., Braaten, D., Jordan, T.A., Fretwell, P.T., Damaske, D., 2013. Early East Antarctic Ice Sheet growth recorded in the landscape of the Gamburtsev Subglacial Mountains. Earth Planet. Sci. Lett. 375, 1–12. doi:10.1016/j.epsl.2013.03.053

Sandiford, M., Quigley, M., de Broekert, P., Jakica, S., 2009. Tectonic framework for the Cenozoic cratonic basins of Australia. Aust. J. Earth Sci. 56, S5–S18. doi:10.1080/08120090902870764

Scheinert, M., Ferraccioli, F., Schwabe, J., Bell, R., Studinger, M., Damaske, D., Jokat, W., Aleshkova, N., Jordan, T., Leitchenkov, G., Blankenship, D.D., Damiani, T.M., Young, D., Cochran, J.R., Richter, T.D., 2016. New Antarctic gravity anomaly grid for enhanced geodetic and geophysical studies in Antarctica. Geophys. Res. Lett. 43, 600–610.

doi:10.1002/2015GL067439

Scher, H.D., Bohaty, S.M., Zachos, J.C., Delaney, M.L., 2011. Two-stepping into the icehouse: East Antarctic weathering during progressive ice-sheet expansion at the Eocene-Oligocene transition. Geology 39, 383–386. doi:10.1130/G31726.1

Scherer, R.P., Aldahan, A., Tulaczyk, S., Possnert, G., Engelhardt, H., Kamb, B., 1998. Pleistocene Collapse of the West Antarctic Ice Sheet. Science 281, 82–85. doi:10.1126/science.281.5373.82

Schoof, C., 2007. Ice sheet grounding line dynamics: Steady states, stability, and hysteresis. J. Geophys. Res. 112, F03S28. doi:10.1029/2006JF000664

Schroeder, D.M., Dowdeswell, J.A., Siegert, M.J., Bingham, R.G., Chu, W., MacKie, E.J., Siegfried, M.R., Vega, K.I., Emmons, J.R., Winstein, K., 2019. Multidecadal observations of the Antarctic ice sheet from restored analog radar records. Proc. Natl. Acad. Sci. 116, 18867–18873. doi:10.1073/pnas.1821646116

Seroussi, H., Ivins, E.R., Wiens, D.A., Bondzio, J., 2017. Influence of a West Antarctic mantle plume on ice sheet basal conditions. J. Geophys. Res. Solid Earth 122, 7127–7155. doi:10.1002/2017JB014423

Shen, W., Wiens, D.A., Anandakrishnan, S., Aster, R.C., Gerstoft, P., Bromirski, P.D., Hansen, S.E., Dalziel, I.W.D., Heeszel, D.S., Huerta, A.D., Nyblade, A.A., Stephen, R., Wilson, T.J., Winberry, J.P., 2018. The Crust and Upper Mantle Structure of Central and West Antarctica From Bayesian Inversion of Rayleigh Wave and Receiver Functions. J. Geophys. Res. Solid Earth 123, 7824–7849. doi:10.1029/2017JB015346

Shen, W., Wiens, D.A., Stern, T., Anandakrishnan, S., Aster, R.C., Dalziel, I., Hansen, S., Heeszel, D.S., Huerta, A., Nyblade, A., Wilson, T.J., Winberry, J.P., 2017. Seismic evidence for lithospheric foundering beneath the southern Transantarctic Mountains, Antarctica. Geology 46, 1–4. doi:10.1130/G39555.1

Siddoway, C.S., Richard, S.M., Fanning, C.M., Luyendyk, B.P., 2004. Origin and emplacement of a middle Cretaceous gneiss dome, Fosdick Mountains, West Antarctica. Spec. Pap. Geol. Soc. Am. 380, 267–294. doi:10.1130/0-8137-2380-9.267

Spiegel, C., Lindow, J., Kamp, P.J.J., Meisel, O., Mukasa, S., Lisker, F., Kuhn, G., Gohl, K., 2016. Tectonomorphic evolution of Marie Byrd Land – Implications for Cenozoic rifting activity and onset of West Antarctic glaciation. Glob. Planet. Change 145, 98–115. doi:10.1016/j.gloplacha.2016.08.013

Stern, T.A., Baxter, A.K., Barrett, P.J., 2005. Isostatic rebound due to glacial erosion within the Transantarctic Mountains. Geology 33, 221–224. doi:10.1130/G21068.1

Stern, T.A., ten Brink, U.S., 1989. Flexural uplift of the Transantarctic Mountains. J. Geophys.

Res. 94, 10315–10330. doi:10.1029/JB094iB08p10315

Studinger, M., Bell, R.E., Blankenship, D.D., Finn, C.A., Arko, R.A., Morse, D.L., Joughin, I., 2001. Subglacial sediments: A regional geological template for ice flow in West Antarctica. Geophys. Res. Lett. 28, 3493–3496. doi:10.1029/2000GL011788

Studinger, M., Bell, R.E., Buck, W.R., Karner, G.D., Blankenship, D.D., 2004. Sub-ice geology inland of the Transantarctic Mountains in light of new aerogeophysical data. Earth Planet. Sci. Lett. 220, 391–408. doi:10.1016/S0012-821X(04)00066-4

Studinger, M., Miller, H., 1999. Crustal structure of the Filchner-Ronne Shelf and Coats Land, Antarctica, from gravity and magnetic data: Implications for the breakup of Gondwana. J. Geophys. Res. Solid Earth 104, 20379–20394. doi:10.1029/1999JB900117

Stump, E., Sheridan, M.F., Borg, S.G., Sutter, J.F., 1980. Early Miocene Subglacial Basalts, the East Antarctic Ice Sheet, and Uplift of the Transantarctic Mountains. Science 207, 757–759. doi:10.1126/science.207.4432.757

Sugden, D.E., Denton, G.H., 2004. Cenozoic landscape evolution of the Convoy Range to Mackay Glacier area, Transantarctic Mountains: Onshore to offshore synthesis. Geol. Soc. Am. Bull. 116, 840–857. doi:10.1130/B25356.1

Sugden, D.E., Jamieson, S.S.R., 2018. The pre-glacial landscape of Antarctica. Scottish Geogr. J. 134, 203–223. doi:10.1080/14702541.2018.1535090

Sugden, D.E., John, B.S., 1976. Glaciers and Landscape. Edward Arnold, London.

Sutherland, R., Spasojevic, S., Gurnis, M., 2010. Mantle upwelling after Gondwana subduction death explains anomalous topography and subsidence histories of eastern New Zealand and west Antarctica. Geology 38, 155–158. doi:10.1130/G30613.1

Taylor, J., Siegert, M.J., Payne, A.J., Hubbard, B., 2004. Regional-scale bed roughness beneath ice masses: Measurement and analysis. Comput. Geosci. 30, 899–908. doi:10.1016/j.cageo.2004.06.007

ten Brink, U.S., Hackney, R.I., Bannister, S., Stern, T.A., Makovsky, Y., 1997. Uplift of the Transantarctic Mountains and the bedrock beneath the East Antarctic ice sheet. J. Geophys. Res. Solid Earth 102, 27603–27621. doi:10.1029/97jb02483

Thomas, R.H., 1979. The dynamics of marine ice sheets. J. Glaciol. 24, 167–177.

Thomson, S.N., Reiners, P.W., Hemming, S.R., Gehrels, G.E., 2013. The contribution of glacial erosion to shaping the hidden landscape of East Antarctica. Nat. Geosci. 6, 203–207. doi:10.1038/ngeo1722

Tinto, K.J., Padman, L., Siddoway, C.S., Springer, S.R., Fricker, H.A., Das, I., Caratori Tontini,

F., Porter, D.F., Frearson, N.P., Howard, S.L., Siegfried, M.R., Mosbeux, C., Becker, M.K., Bertinato, C., Boghosian, A., Brady, N., Burton, B.L., Chu, W., Cordero, S.I., Dhakal, T., Dong, L., Gustafson, C.D., Keeshin, S., Locke, C., Lockett, A., O'Brien, G., Spergel, J.J., Starke, S.E., Tankersley, M., Wearing, M.G., Bell, R.E., 2019. Ross Ice Shelf response to climate driven by the tectonic imprint on seafloor bathymetry. Nat. Geosci. doi:10.1038/s41561-019-0370-2

Tochilin, C.J., Reiners, P.W., Thomson, S.N., Gehrels, G.E., Hemming, S.R., Pierce, E.L., 2012. Erosional history of the Prydz Bay sector of East Antarctica from detrital apatite and zircon geo- and thermochronology multidating. Geochemistry, Geophys. Geosystems 13, 1–21. doi:10.1029/2012GC004364

Tripati, A., Backman, J., Elderfield, H., Ferretti, P., 2005. Eocene bipolar glaciation associated with global carbon cycle changes. Nature 436, 341–346. doi:10.1038/nature04289

van Wijk, J.W., Lawrence, J.F., Driscoll, N.W., 2008. Formation of the Transantarctic Mountains related to extension of the West Antarctic Rift system. Tectonophysics 458, 117–126. doi:10.1016/j.tecto.2008.03.009

van Wyk de Vries, M., Bingham, R.G., Hein, A.S., 2018. A new volcanic province: an inventory of subglacial volcanoes in West Antarctica. Geol. Soc. London, Spec. Publ. 461, 231–248. doi:10.1144/SP461.7

Watts, A.B., 2001. Isostasy and Flexure of the Lithosphere. Cambridge University Press, Cambridge.

Watts, A.B., Burov, E.B., 2003. Lithospheric strength and its relationship to the elastic and seismogenic layer thickness. Earth Planet. Sci. Lett. 213, 113–131. doi:10.1016/S0012-821X(03)00289-9

Watts, A.B., Moore, J.D.P., 2017. Flexural Isostasy: Constraints From Gravity and Topography Power Spectra. J. Geophys. Res. Solid Earth 122, 1–14. doi:10.1002/2017JB014571

Watts, A.B., Zhong, S.J., Hunter, J., 2013. The Behavior of the Lithosphere on Seismic to Geologic Timescales. Annu. Rev. Earth Planet. Sci. 41, 443–468. doi:10.1146/annurev-earth-042711-105457

Weissel, J.K., Karner, G.D., 1989. Flexural uplift of rift flanks due to mechanical unloading of the lithosphere during extension. J. Geophys. Res. Solid Earth 94, 13919–13950. doi:10.1029/JB094iB10p13919

Wenman, C.P., Harry, D.L., Jha, S., 2020. Post Middle Miocene Tectonomagmatic and Stratigraphic Evolution of the Victoria Land Basin, West Antarctica. Geochemistry, Geophys. Geosystems 21. doi:10.1029/2019GC008568

White, D.A., 2013. Cenozoic landscape and ice drainage evolution in the Lambert Glacier-

Amery Ice Shelf system. Geol. Soc. London, Spec. Publ. 381, 151–165. doi:10.1144/SP381.15

Whittaker, J.M., Müller, R.D., Gurnis, M., 2010. Development of the Australian-Antarctic depth anomaly. Geochemistry, Geophys. Geosystems 11. doi:10.1029/2010GC003276

Wilson, D.S., Jamieson, S.S.R., Barrett, P.J., Leitchenkov, G., Gohl, K., Larter, R.D., 2012. Antarctic topography at the Eocene-Oligocene boundary. Palaeogeogr. Palaeoclimatol. Palaeoecol. 335–336, 24–34. doi:10.1016/j.palaeo.2011.05.028

Wilson, D.S., Luyendyk, B.P., 2009. West Antarctic paleotopography estimated at the Eocene-Oligocene climate transition. Geophys. Res. Lett. 36, L16302. doi:10.1029/2009GL039297

Wilson, D.S., Luyendyk, B.P., 2006. Bedrock platforms within the Ross Embayment, West Antarctica: Hypotheses for ice sheet history, wave erosion, Cenozoic extension, and thermal subsidence. Geochemistry, Geophys. Geosystems 7, 1–23. doi:10.1029/2006GC001294

Wilson, D.S., Pollard, D., DeConto, R.M., Jamieson, S.S.R., Luyendyk, B.P., 2013. Initiation of the West Antarctic Ice Sheet and estimates of total Antarctic ice volume in the earliest Oligocene. Geophys. Res. Lett. 40, 4305–4309. doi:10.1002/grl.50797

Winberry, J.P., Anandakrishnan, S., 2004. Crustal structure of the West Antarctic rift system and Marie Byrd Land hotspot. Geology 32, 977–980. doi:10.1130/G20768.1

Winterbourne, J., White, N., Crosby, A., 2014. Accurate measurements of residual topography from the oceanic realm. Tectonics 33, 982–1015. doi:10.1002/2013TC003372

Young, D.A., Wright, A.P., Roberts, J.L., Warner, R.C., Young, N.W., Greenbaum, J.S., Schroeder, D.M., Holt, J.W., Sugden, D.E., Blankenship, D.D., van Ommen, T.D., Siegert, M.J., 2011. A dynamic early East Antarctic Ice Sheet suggested by ice-covered fjord landscapes. Nature 474, 72–75. doi:10.1038/nature10114

Zachos, J., Kump, L., 2005. Carbon cycle feedbacks and the initiation of Antarctic glaciation in the earliest Oligocene. Glob. Planet. Change 47, 51–66. doi:10.1016/j.gloplacha.2005.01.001

Zachos, J., Pagani, M., Sloan, L., Thomas, E., Billups, K., 2001. Trends, rhythms, and aberrations in global climate 65 Ma to present. Science 292, 686–693. doi:10.1126/science.1059412

Zachos, J.C., Dickens, G.R., Zeebe, R.E., 2008. An early Cenozoic perspective on greenhouse warming and carbon-cycle dynamics. Nature 451, 279–283. doi:10.1038/nature06588

Zachos, J.C., Flower, B.P., Paul, H., 1997. Orbitally paced climate oscillations across the Oligocene/Miocene boundary. Nature 388, 567–570. doi:10.1038/41528

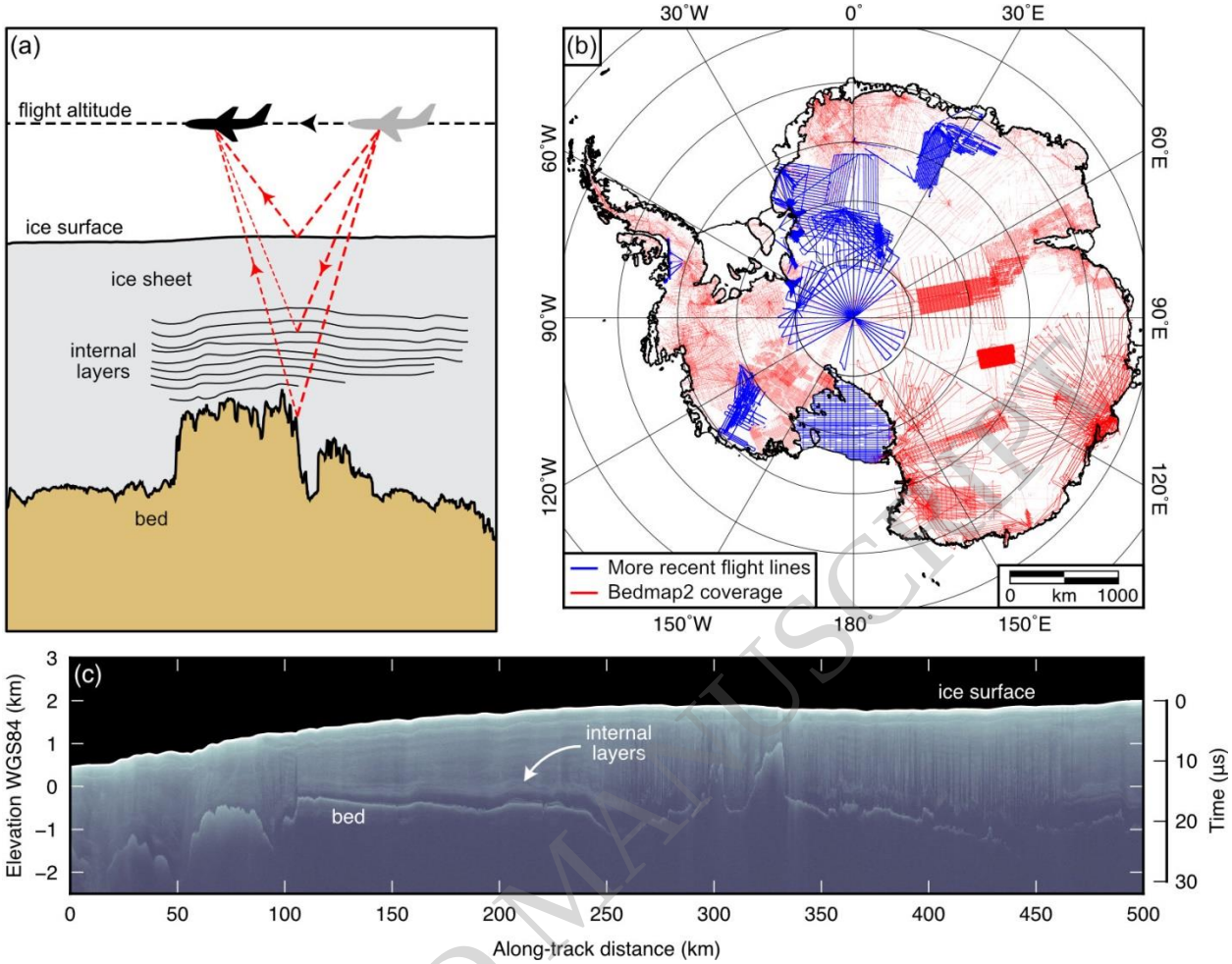

Figure 1

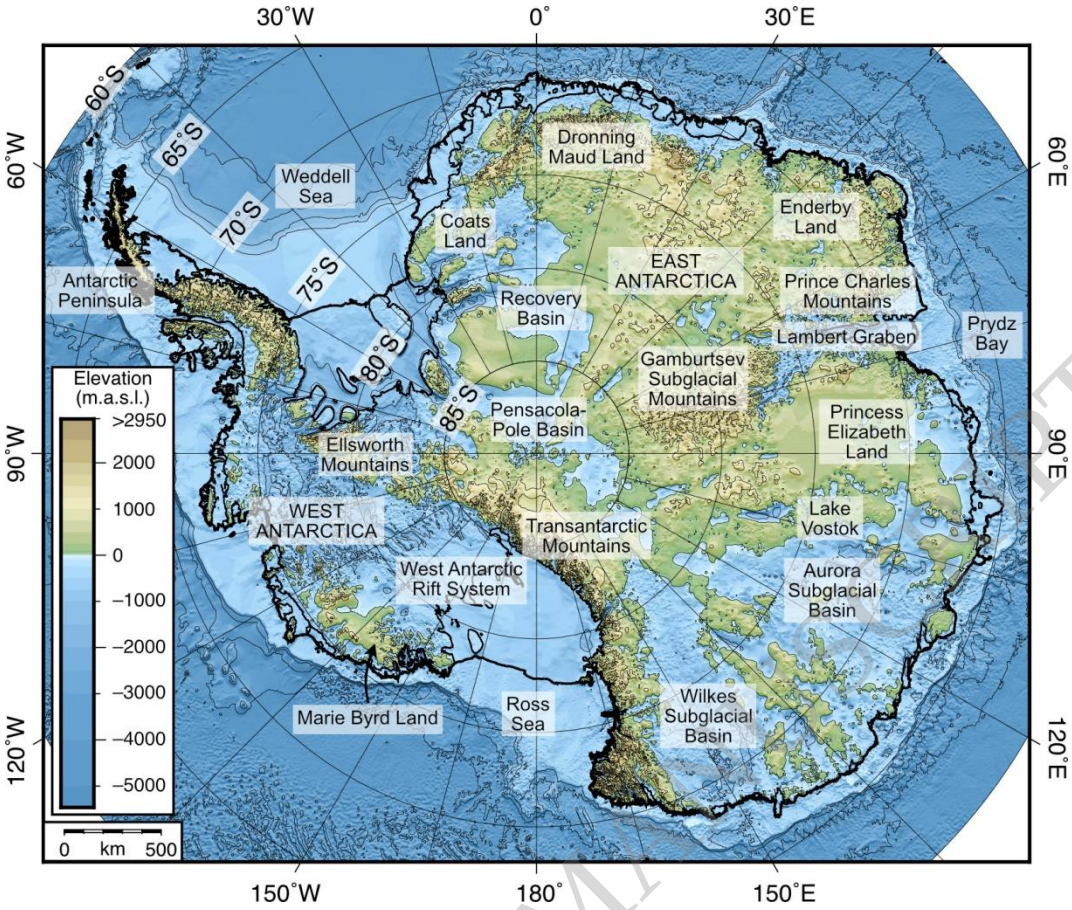

Figure 2

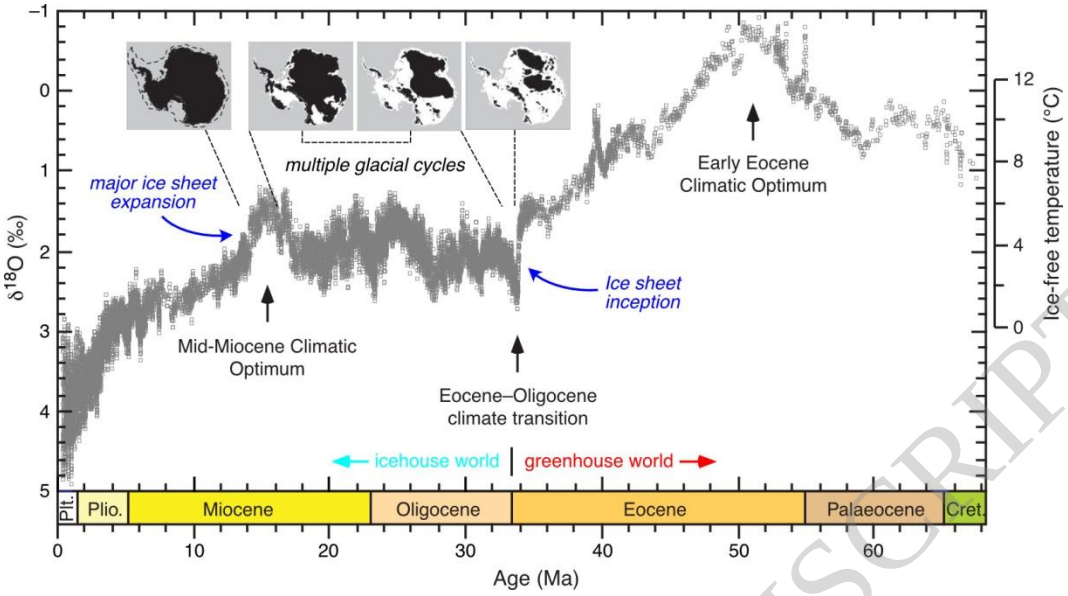

Figure 3

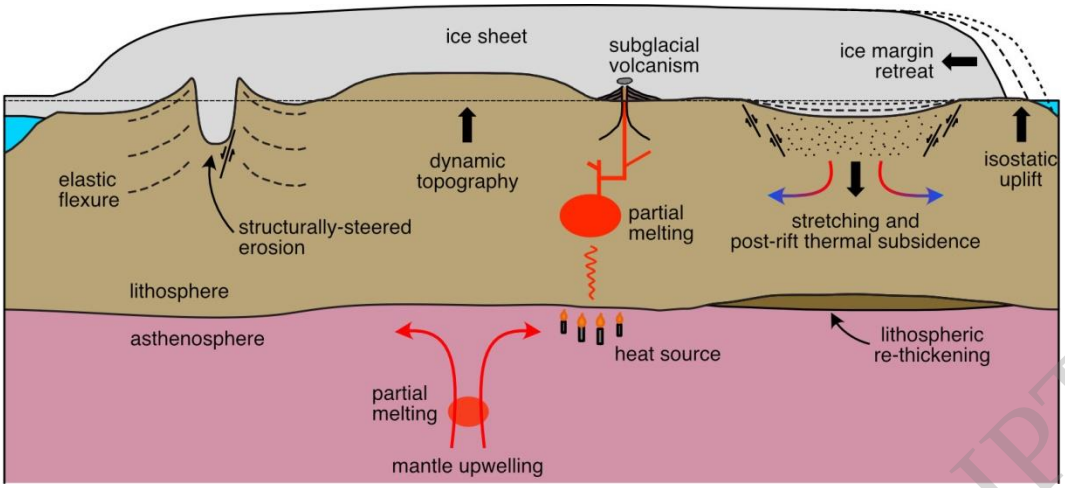

Figure 4

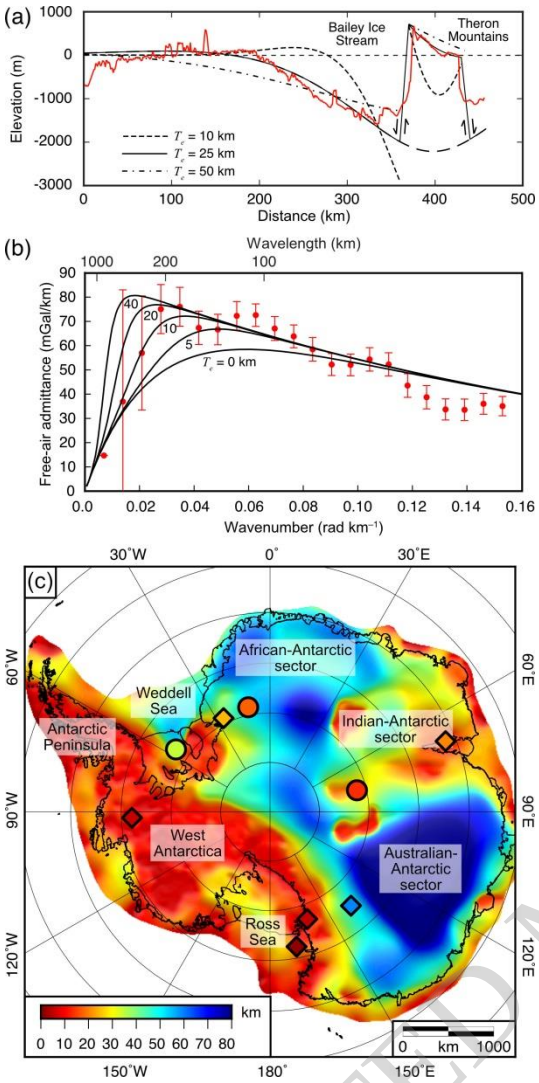

Figure 5

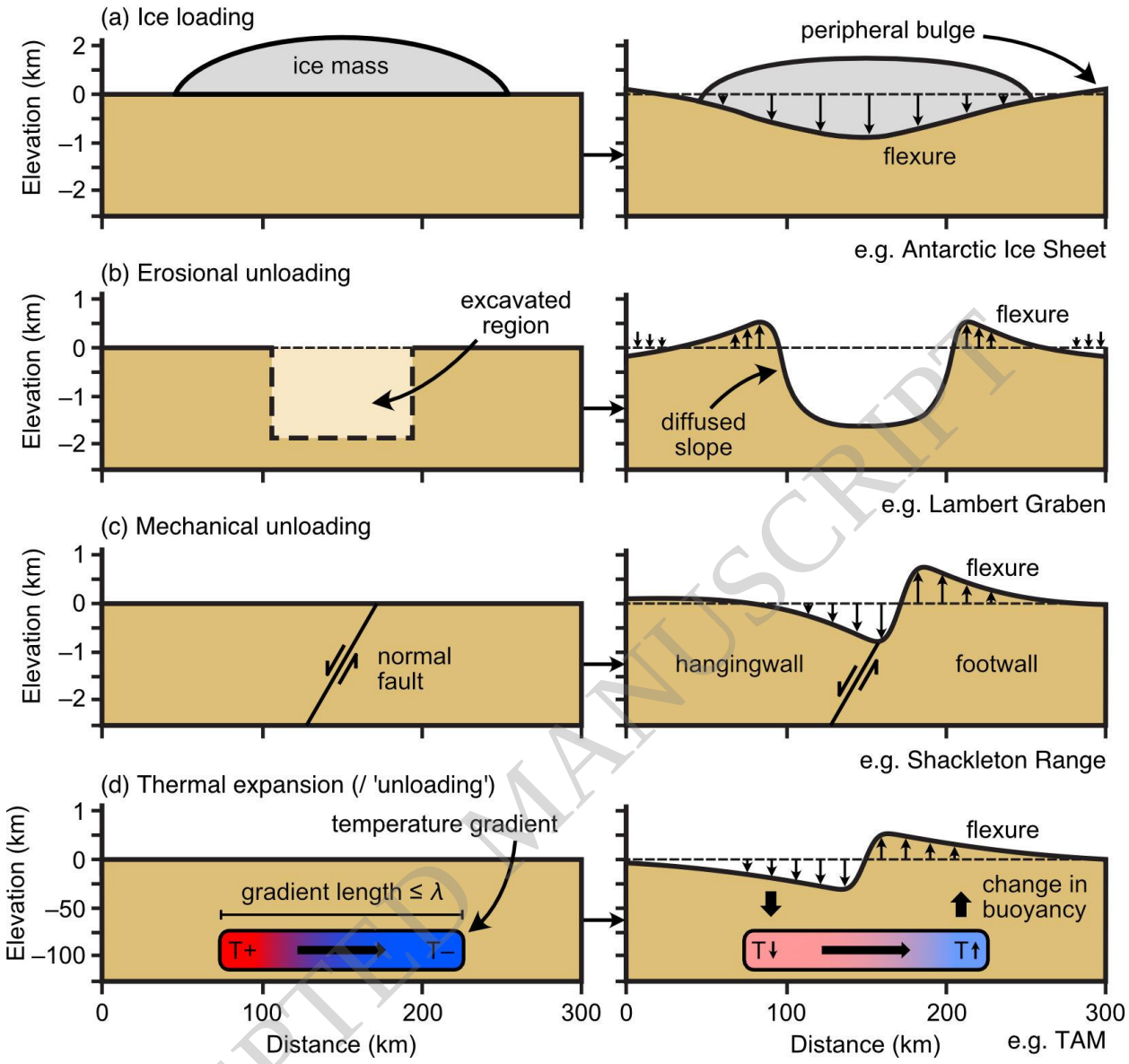

Figure 6

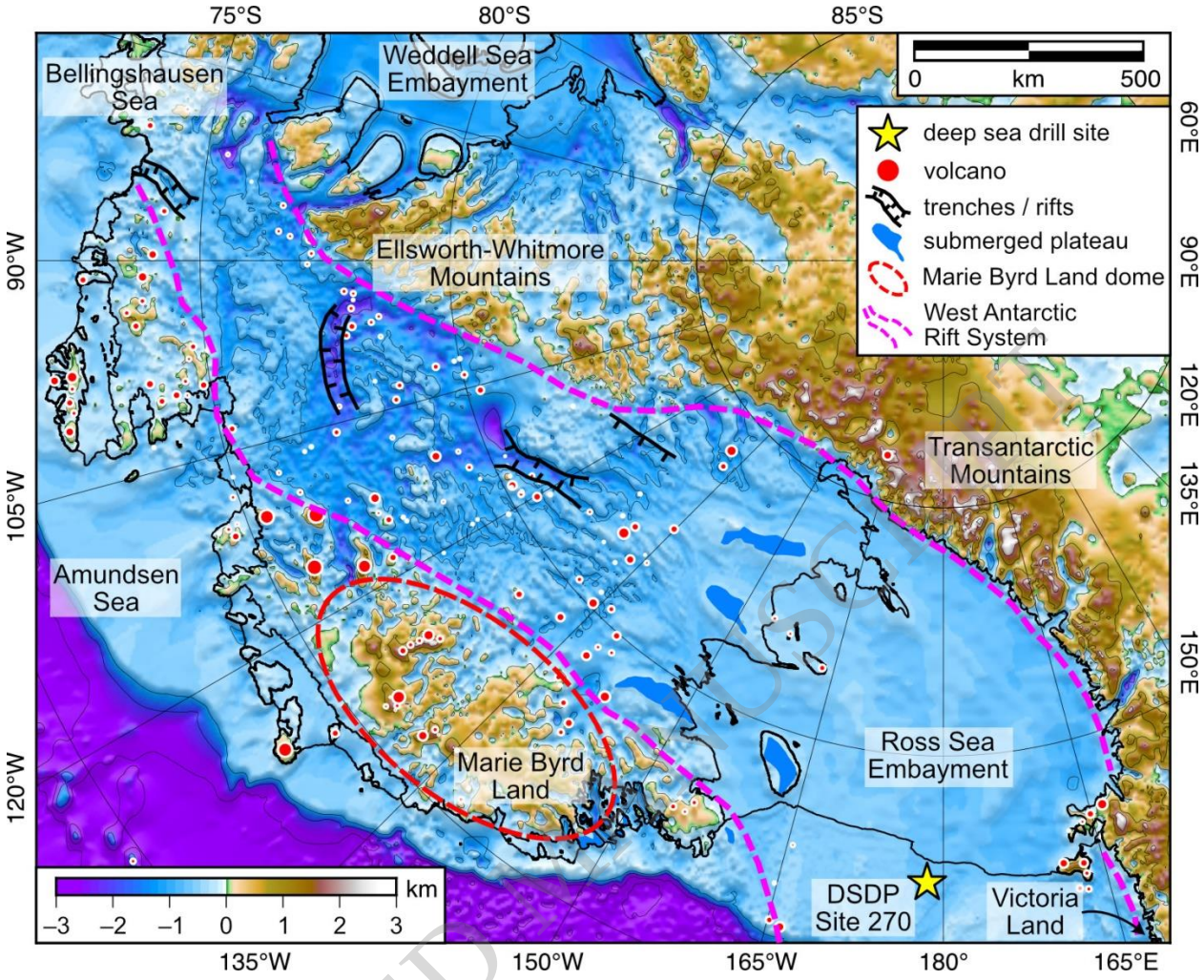

Figure 7

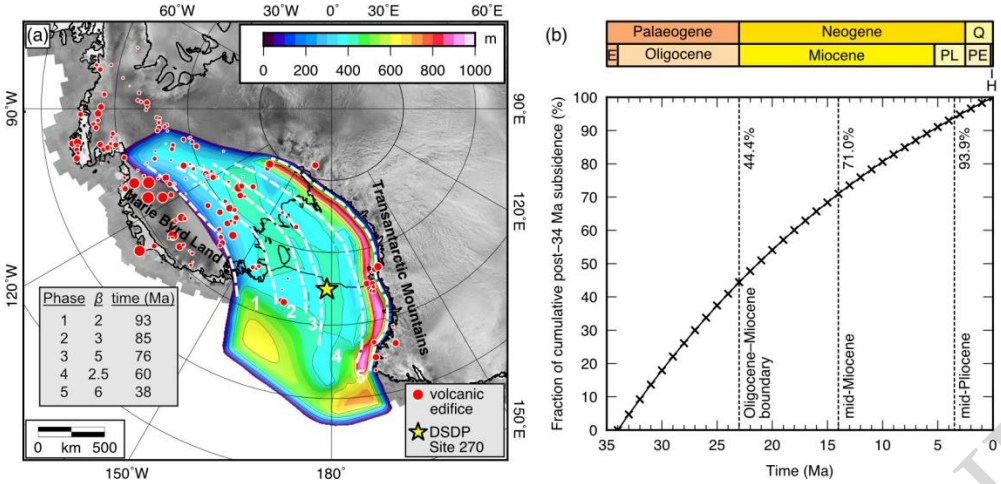

Figure 8

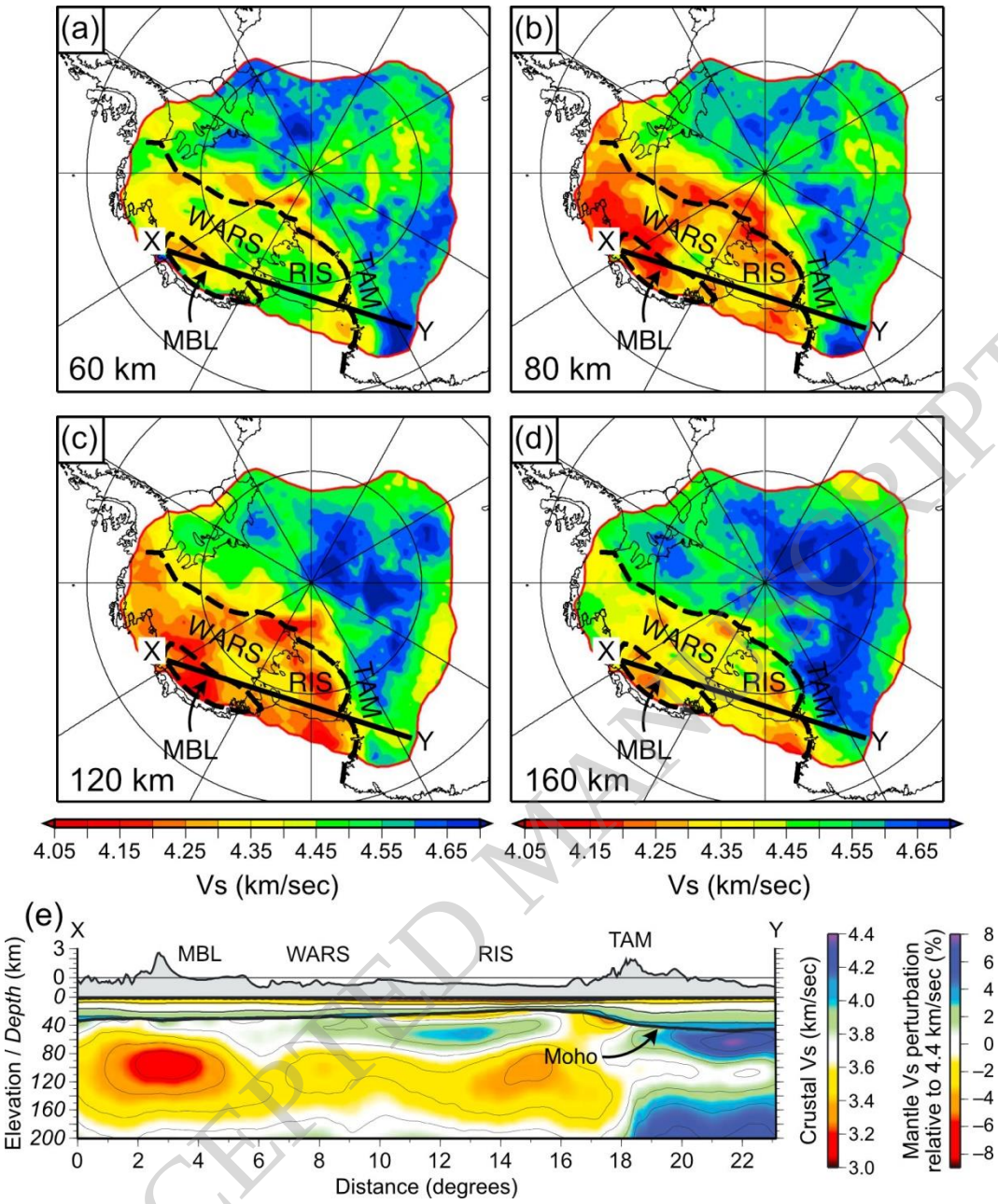

Figure 9

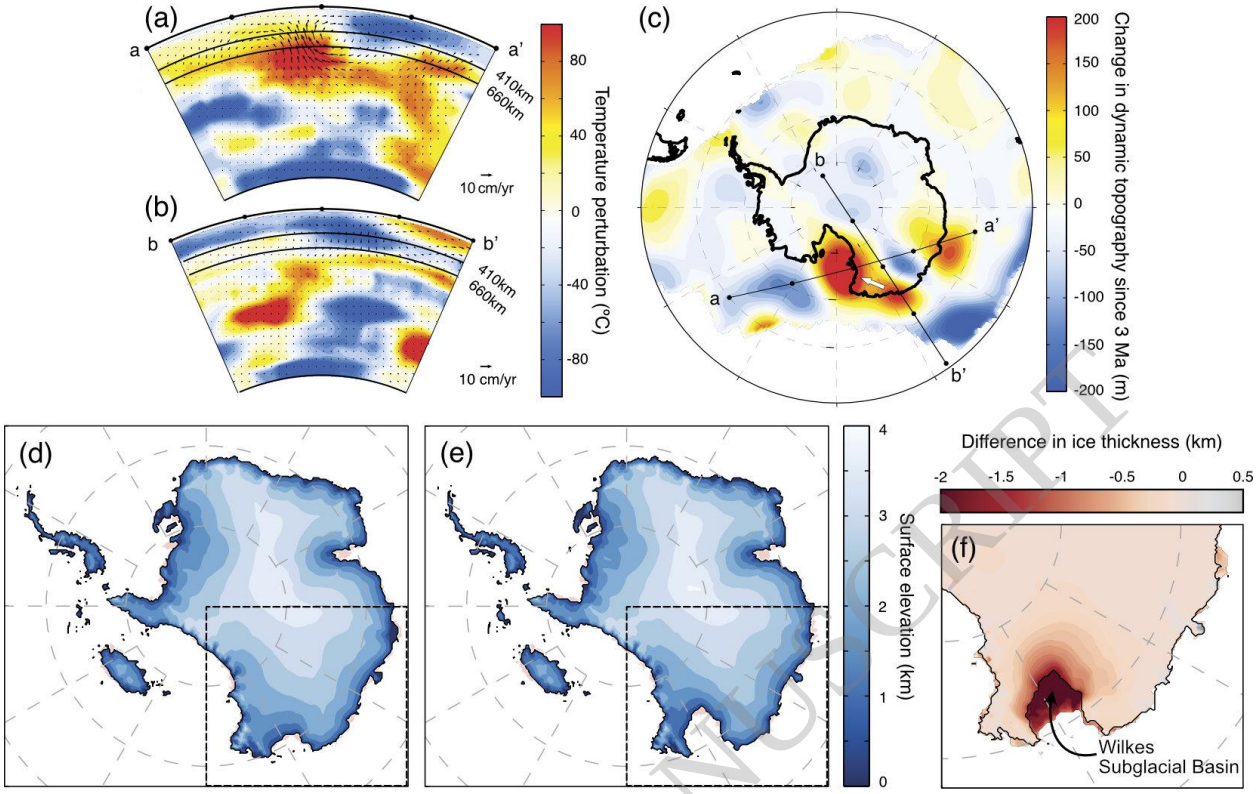

Figure 10

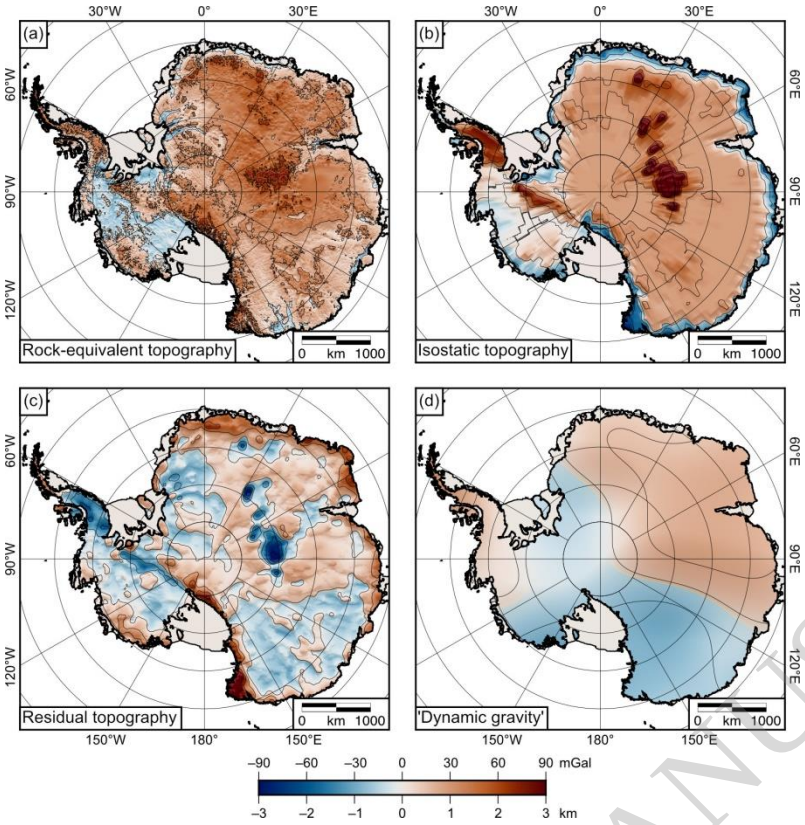

Figure 11